Humanized Monoclonal Antibody IgG1k, NISTmAb RM 8671 Summary of 5 Year Stability Verification (5YSV)

Katharina Yandrofski
John E. Schiel
Trina Mouchahoir
Srivalli Telikepalli
Paul C. DeRose
Alan N. Heckert
Dean C. Ripple
Karen W. Phinney
John P. Marino

NIST | NATIONAL INSTITUTE OF
STANDARDS AND TECHNOLOGY
U.S. DEPARTMENT OF COMMERCE

Humanized Monoclonal Antibody IgG1k, NISTmAb RM 8671 Summary of 5 Year Stability Verification (5YSV)

Katharina Yandrofski
John E. Schiel
Trina Mouchahoir
Srivalli Telikepalli
Dean C. Ripple
Karen W. Phinney
John P. Marino
*Biomolecular Measurement Division
Material Measurement Laboratory*

Paul C. DeRose
*Biosystem and Biomaterials Division
Material Measurement Laboratory*

Alan N. Heckert
*Statistical Engineering Division
Information Technology Laboratory*

NIST SP 260-237
March 2023

Values reported herein were collected during NISTmAb qualification and/or value assignment and are current at the time of publication. Users should always refer to the Report of Investigation (https://www-s.nist.gov/srmors/view_detail.cfm?srm=8671) for their specific material lot for the most up-to-date values and uncertainty ranges. Certain commercial equipment, instruments, software, or materials, commercial or non-commercial, are identified in this paper in order to specify the experimental procedure adequately. Such identification does not imply recommendation or endorsement of any product or service by NIST, nor does it imply that the materials or equipment identified are necessarily the best available for the purpose.

NIST Technical Series Policies
Copyright, Use, and Licensing Statements
NIST Technical Series Publication Identifier Syntax

NIST Author ORCID iDs
Katharina Yandrofski: 0000-0002-0570-8011
John E. Schiel: 0000-0001-5353-3343
Trina Mouchahoir: 0000-0002-6790-830X
Srivalli Telikepalli: 0000-0003-4687-6123
Paul C. DeRose: 0000-0002-1406-633X
Alan N. Heckert: 0000-0002-8430-6757
Dean C. Ripple: 0000-0002-6413-1339
Karen W. Phinney: 0000-0001-7540-5860
John P. Marino: 0000-0002-6860-5853

Abstract

NISTmAb RM 8671 is an IgG1κ monoclonal antibody that has been extensively characterized and released as the first of its kind biopharmaceutical reference material in 2016. This material was intended primarily for use in evaluating the performance of methods for determining physicochemical and biophysical attributes of monoclonal antibodies. It also provides a representative test molecule for development of novel technologies for therapeutic protein characterization. The lifecycle management of NISTmAb includes a long-term stability verification to evaluate the homogeneity and stability for the first 3 lots (14HB-D-001, 14HB-D-002, and 14HB-D-003) of this material. Initial certification to assign property values and confirm identification used a wide variety of analytical methods including UV-Vis spectrophotometry, size exclusion chromatography, capillary electrophoresis, dynamic light scattering, flow imaging, and peptide mapping. Reported here is a summary of these analytical methods and results for the 5-year stability verification (5YSV) for RM 8671 demonstrating the material is homogeneous and stable.

Key words

Reference Material; NISTmAb; Monoclonal Antibody; Biotherapeutic; Biopharmaceutical; System Suitability; Biosimilar

Table of Contents

List of Figures

1. Introduction

The NISTmAb RM 8671 is an IgG1κ monoclonal antibody expressed in murine suspension culture. The material is a ~150 kDa homodimer of two identical light chains and two identical heavy chains linked through both inter and intra-disulfide bonds. The protein has numerous low abundance post-translation modifications including methionine oxidation, deamidation, and glycation. The molecule also has nearly complete N-terminal pyroglutamation and glycosylation of the heavy chains.   These and other product quality attributes were extensively characterized in the ACS book series "State of the Art and Emerging Technologies for Therapeutic Monoclonal Antibody Characterization" [1-3].   This extensive characterization is representative of that which would be expected in the S3.2 characterization section of a biological licensure application [4] for a therapeutic protein. The NISTmAb is not intended for clinical use, however this level of characterization demonstrated the RM material was representative of a typical drug substance in all salient features. Simultaneously, the utility of such a material during the drug development process for activities including analytical method performance evaluation, system suitability control, and development of innovative technologies was demonstrated.   To this end, a first-of-its kind qualitative and quantitative biopharmaceutical Reference Material to supplement drug substance/product characterization was described in a five-paper series [5-8]. The NISTmAb IgG1κ is intended to provide a well characterized, longitudinally available test material that is expected to greatly facilitate development of originator and follow-on biologics for the foreseeable future.

Property values assigned to the first three lots of NISTmAb were reported in the literature as a five paper publication series [5-8]. Herein we provide a long-term stability assessment referred to as the 5-year stability verification (5YSV) of the initial three lots of NISTmAb (lots 14HB-D-001 through 14HB-D-003) to assure continued homogeneity and stability with respect to assigned property values. Each analytical method is described in an individual section below.

2. Stratified Sampling

Samples were randomly selected from the existing stock of Reference Material using a stratified sampling plan. Samples reserved from each lot for stability were reserved as indicated in Table 1 and Figure 1 below.

Table 1. Samples selected for stability assessment.

Rack	Homogeneity UV	Physicochemical Homogeneity
1	1 random	3 same row
10	1 random	
20	1 random	
30	1 random	

40	1 random	
50	1 random	3 same row
60	1 random	
70	1 random	
80	1 random	
90	1 random	3 same row
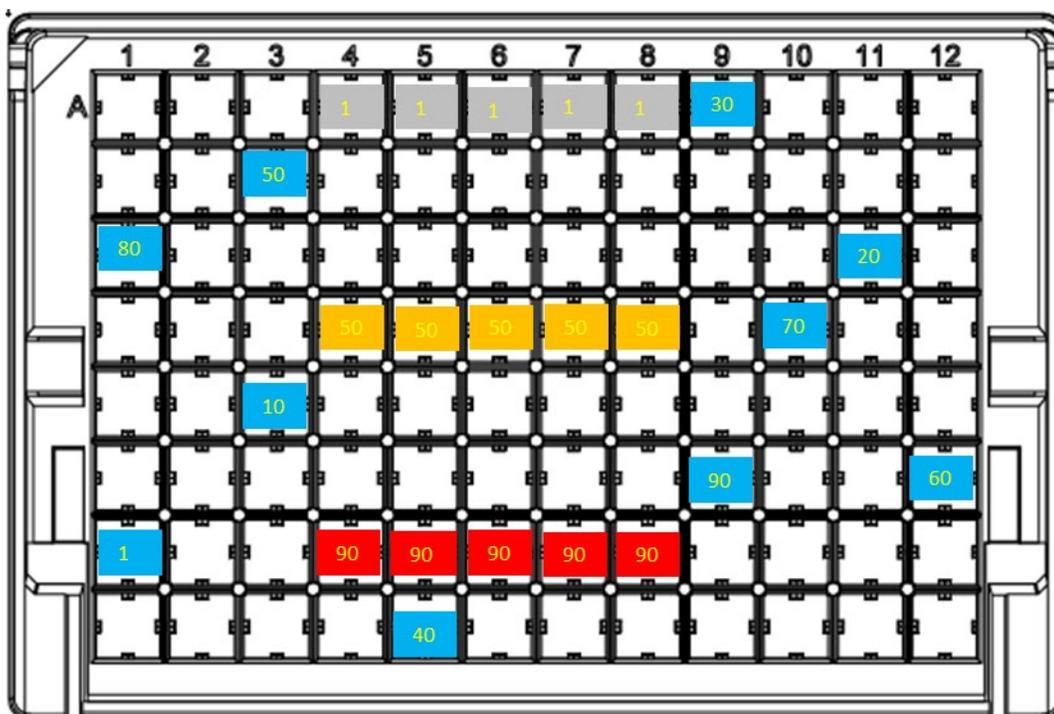
Figure 1. Representative matrix rack sampling pattern for homogeneity assessment.
Note actual rack numbers and positions chosen at random. "Blue" samples were reserved from the respective rack for UV and samples represented by other colors were reserved for physiochemical assessment.

2.1.1. UV Samples

A total of ten (10) samples from each lot were reserved for stability assessment as depicted in Table 1 and Figure 1. Vials from rows/columns were chosen at random from racks across the fill sequence. No further sample preparation was required for these samples. They were stored at -80 °C and further handling and analysis is described in the pertinent section below.

2.1.2. Physicochemical Homogeneity Samples

A total of nine (9) samples were reserved for physicochemical stability assessment from each lot as depicted in Table 1 and Figure 1. One vial from each lot/rack (1, 50, and 90) was thawed at room temperature for a total of nine (9) vials). Each 800 µL vial was aliquoted into 5 x 150 µL fractions into a clean Thermo Matrix 1 mL tube. The fractions were then frozen at -80 °C and stored until analysis. Three vials from each lot/rack (1, 50, and 90) were used for particulate and DLS measurements for a total of 27 physicochemical homogeneity vials. One vial from each lot/rack (1, 50, and 90) was retained as a set of backup samples if required, for a total of 9 physicochemical homogeneity vials.

3. Statistical Analysis

Each analytical method used was originally qualified in 2016 using Primary Sample 8670, a developmental lot of RM 8671. The results of which were used to set method performance criteria, such that PS 8670 could be used as a system suitability control [1-4]. The total variance of an analytical method performed on 8670 was:

$$u_{c,8670}^2 = u_{r,8670}^2 + u_{other,8670}^2 \tag{1}$$

Where $u_{c,8670}$ represents the combined standard uncertainty at the level of one standard deviation. A one-way nested ANOVA was used to split the measured variances into "within group" (or repeatability, $u^2_{r,8670}$) and "between group" ($u^2_{other,8670}$) contributions to the total variance, which included limited intermediate precision elements such as column, day, buffer lot, etc., but not different analysis or instruments).

In the original RM 8671 value assignment, it was assumed that intermediate precision contributions (e.g. between column, inter-day, etc.) to total variance for RM 8671 were identical to that of PS 8670[5].

$$u_{other,70}^2 = u_{other,71}^2 = u_{other}^2 \tag{2}$$

Homogeneity of each RM 8671 lot was evaluated via a series of measurements performed on the same day to provide the inter-vial uncertainty, $u^2_{iv,71}$, a Type A contribution to uncertainty for RM 8671.
u_{other}^2 was incorporated as B-Type uncertainty, as it is a reference value from previous PS 8670 method qualification intended to incorporate historical method experience [2]
 The combined standard uncertainty for RM 8671 ($u^2_{c,71}$), reported at the level of one standard deviation, was therefore given by equation 3.

$$\therefore u_{c,71}^2 = u_{iv,71}^2 + u_{other}^2 \tag{3}$$

In the current dataset, samples were analyzed according to previously qualified methods and evaluated for conformance to specification. Control charts were prepared with the control range taken as the mean from the 2016 qualification and/or value assignment ± the expanded uncertainty for that measurement (±2uc for UV and ±3uc for physicochemical assays). Each lot was treated individually. The material was considered to be stable and homogeneous when the 2021 results fell within this expanded uncertainty range for an individual lot/method.

DLS measurements were not assigned uncertainty ranges in the initial 2016 certification, however they were added in the 5YSV to meet the new formatting criteria for the Reference Material Information Sheet (RMIS)[6]. Uncertainty ranges were calculated as described in equations 1 and 2 and as previously published. [5]

No modifications to the control chart protocol were required for methods other than capillary electrophoresis methods. Capillary electrophoresis methods (CZE, nrCE-SDS, rCE-SDS) demonstrated minor shifts in performance observed for all samples (IQ, PS 8670, and RM 8671) due to long-term intermediate precision contributions to uncertainty that were immeasurable during the first value assignment (performed over a limited time and one analyst). We now have long term data for RM 8671 that includes potential contributions from inter-analyst variability as well as long-term variation in method consumables (i.e. gel lots, capillaries, and equipment age). Inter-analyst variability was considered as a new factor and a new two-way ANOVA was conducted on the PS 8670 and RM 8671 data from 2016 and 5YSV. This provided a new inter-analyst uncertainty (u_{analyst}) for each lot.   All current lots of RM 8671 were derived from the same original batch and the same two analysts conducted the analysis on each lot. The largest u_{analyst} determined for an individual lot was applied to all lots as a constant to allow use for future RM value assignment activities. The new uncertainty for the material would be:

$$\therefore u_{c,71}^2 = u_{iv,71}^2 + u_{\text{other},70}^2 + u_{\text{analyst}}^2 \tag{4}$$

Note, uncertainty estimates were only expanded for CE-based methods, i.e. only methods for which it appears a long-term variability appeared to affect method performance/integration, but no new peaks appear present. It is likely that future stability evaluations may need to be done on different instruments, analysts etc. In this case a new factor and B-type uncertainty component such as $u_{\text{instrument}}$ could be added.

A new two-way ANOVA was also conducted on the PS 8670 data from 2016 and 5YSV for all capillary electrophoresis methods to establish new performance criteria to account for the minor shifts in performance due to intermediate precision contributions as described above. The current performance criteria for PS 8670 are listed below for all capillary electrophoresis methods.

The criteria for injections of PS 8670 under non-reducing conditions are as follows:

- Visually conforms to expectation (expected peak shape, no new peaks above LOD).

- 10 kDa internal standard migration time falls within $\pm 3u_c$ of the mean: (11.85 min to 12.97 min).
- Monomer migration time falls within $\pm 3u_c$ of the mean: (26.19 min to 29.87 min).
- Monomeric purity falls within $\pm 3u_c$ of the mean: (97.74 % to 99.94 %).

The criteria for injections of PS 8670 under reducing conditions are as follows:

- Visually conforms to expectation (expected peak shape, no new peaks above LOD).
- 10 kDa internal standard migration time falls within $\pm 3u_c$ of the mean: (11.85 min to 12.97 min).
- Heavy chain migration time falls within $\pm 3u_c$ of the mean: (18.40 min to 20.16 min).
- Heavy chain relative abundance falls within $\pm 3u_c$ of the mean: (66.63 % to 67.87 %).

The criteria for injections of PS 8670 for capillary zone electrophoresis are as follows:

- Visually conforms to expectation (expected peak shape and pattern)
- The migration time of the main peak falls within $\pm 3u_c$ of the mean (8.26 min to 11.02 min)
- The Main group RA (%) falls within $\pm 3u_c$ of the mean: (73.53 % to 75.82 %).

4. Non-Certified Value Stability Evaluation

NIST non-certified values are best estimates based on currently available information and were referred to as "Reference Values" or "Informational Values" from 1987 until July 2020[6]. Non-certified values are suitable for use in method development, method harmonization, and process control, but may not provide metrological traceability to the International System of Units (SI) or other higher-order reference system. These values must meet the three criteria of measurand, homogeneity, and stability, but additional attributes such as accuracy and traceability may not be adequately established. [6] In addition, the value must include an associated uncertainty representing repeatability, homogeneity, precision, etc.[6]

Values for RM 8671 were initially assigned as documented in a series of publications in 2018 along this a thorough expansion on the specific protocols and results. [1-5]. Physicochemical attributes of RM 8671 were measured using NIST traceable UV Vis Spectrophotometry and qualified size exclusion chromatography (SEC), capillary sodium dodecyl sulfate electrophoresis (CE-SDS), capillary zone electrophoresis (CZE), and dynamic light scattering (DLS) methods[2, 3, 5]. These analytical assays were qualified using the primary sample (PS) in order to establish method performance criteria. Qualification exercises were modeled after the ICH Q2(R1) guidelines for method validation and included assessment of linearity, limit of detection (LOD)/limit of quantification (LOQ), range, and precision (repeatability and some intermediate precision).

Measurements described in the current publication were conducted with the highest degree of sameness possible (same instrumentation, consumables, analytical method, etc.), including bracketing each analysis with an instrument qualification (IQ) standard and the PS to ensure

system suitability. Both the IQ standard and PS were required to pass pre-defined method performance criteria derived from method qualification. Any changes to analytical procedures and/or non-certified values or associated uncertainties are detailed in the respective method sections below. All values documented in this special publication and corresponding RMIS (https://shop.nist.gov/ccrz__ProductDetails?sku=8671&cclcl=en_US) are identified as non-certified values unless otherwise stated.

4.1. Mass Concentration Non-Certified Value Assignment

4.1.1. Method

UV absorbance spectrophotometry was used to confirm stability of the decadic attenuance values of each RM 8671 lot. Concentration of protein material is often determined using UV-Visible spectrophotometry wherein the measured absorbance is assumed to be equivalent to the total decadic attenuance. The decadic attenuance, D, is computed as the negative logarithm (base 10) of the transmittance, and is analogous to absorbance except for the inclusion of scattering and luminescence effects upon the radiant power exiting the sample [9]. Concentrations reported in the current publications are based on decadic attenuance at 280 nm (D280) to most adequately reflect the measurements that will be performed on this material by the end user [5]. Although the use of decadic attenuance results in an "apparent concentration", it is most reflective of the experiments that will be performed by the end user.

Decadic attenuance measurements on the 5YSV samples were performed using the same instrument, cuvette, and analytical method as described in previously [5]. Briefly, Primary decadic attenuance measurements of the mAb was measured using the MML Transfer Spectrophotometer (Cary 6000i spectrometer (Agilent)), which is traceable to the national reference instrument for absorbance (HAS-2). The concentration was determined for each of ten (10) vials from an individual lot based on equation 5.

$$C = \frac{D_{corr}}{\varepsilon \cdot b} \tag{5}$$

Concentration of the NISTmAb was determined utilizing a theoretical extinction coefficient (ε) of 1.42 (mL mg^{-1} cm^{-1}) and the pathlength of the UV cuvette (b = 0.5092 mm) after subtracting decadic attenuance values of a Formulation Buffer Blank using the same cuvette.

4.1.2. Qualitative Results

A representative UV absorbance spectrum overlaying the 2016 results with the 5YSV samples is shown in Figure 2 (corrected for buffer background).
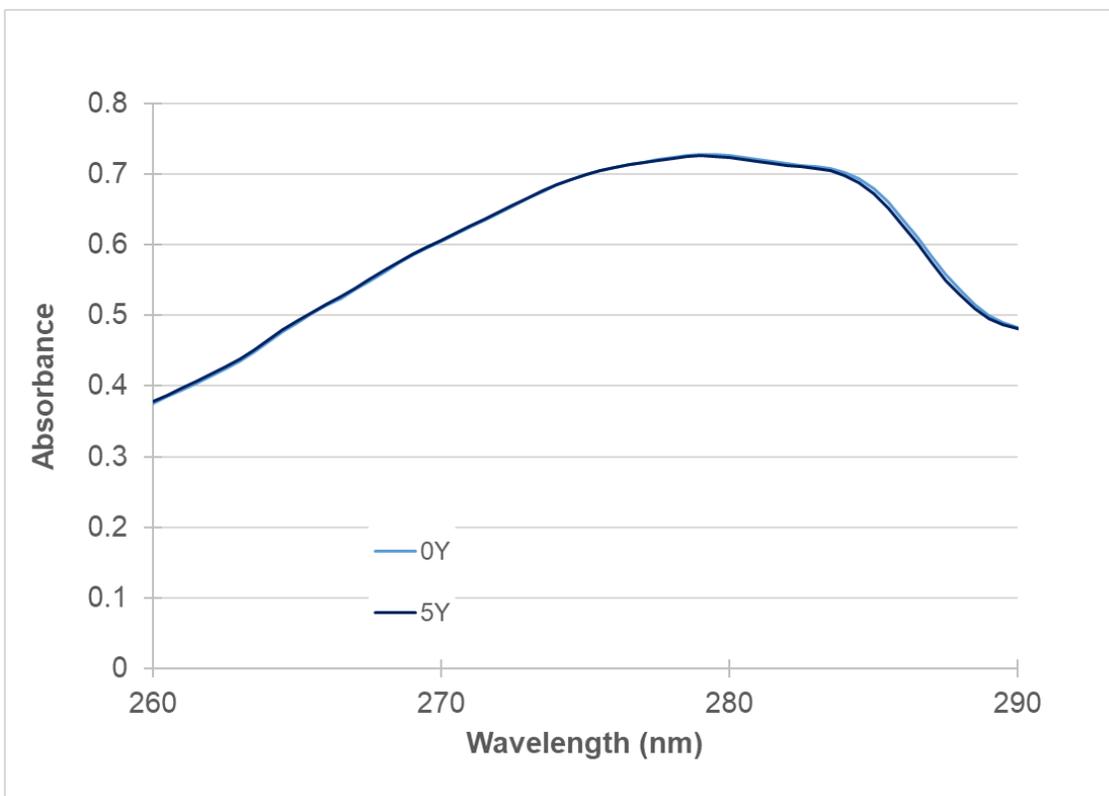
Figure 2. Representative UV absorbance spectrum comparison for lot 14HB-D-002.

The spectral properties for lots 14HB-D-001 and 14HB-D-002 were consistent in all salient features with those obtained in 2016. The peak maximum position and magnitude are also consistent for 14HB-D-001 and 14HB-D-002. The peak position for lot 3 is shifted by approximately 0.5 nm, corresponding to one step interval for wavelength. The 5YSV lot 3 spectra are consistent in peak maximum position and magnitude to those of lots 1 and 2 from both 2016 (0y) and 5YSV (5y). This implies that the lot 3 spectra from 2016 were inadvertently shifted by approximately -0.5 nm relative to the technically correct spectrum due to a calibration error. In order to be consistent with lots 1 and 2, the lot 3 2016 concentration and uncertainty values were recalculated using the absorbance value measured at 279.5 nm, which in actuality is 280 nm due to the calibration error on that day.

4.1.3. Quantitative Results

Mass concentration control charts for each lot are depicted in Figure 3, with the control range taken as the mean mass concentration ± two times the combined standard uncertainty ($\pm 2u_c$) determined in 2016 [5]. Individual data points for each measurement from 2016 and 5YSV are shown for lots 14HB-D-001, 14HB-D-002, and 14HB-D-003 respectively. All values for lots are shown to be within the control range (grey bars) for each lot; the material is still homogeneous and stable with respect to mass concentration, resulting in no change to the

reference values or uncertainty. Due to the calibration wavelength error from the 2016 certification, reference values and ranges were shifted for lot 3.
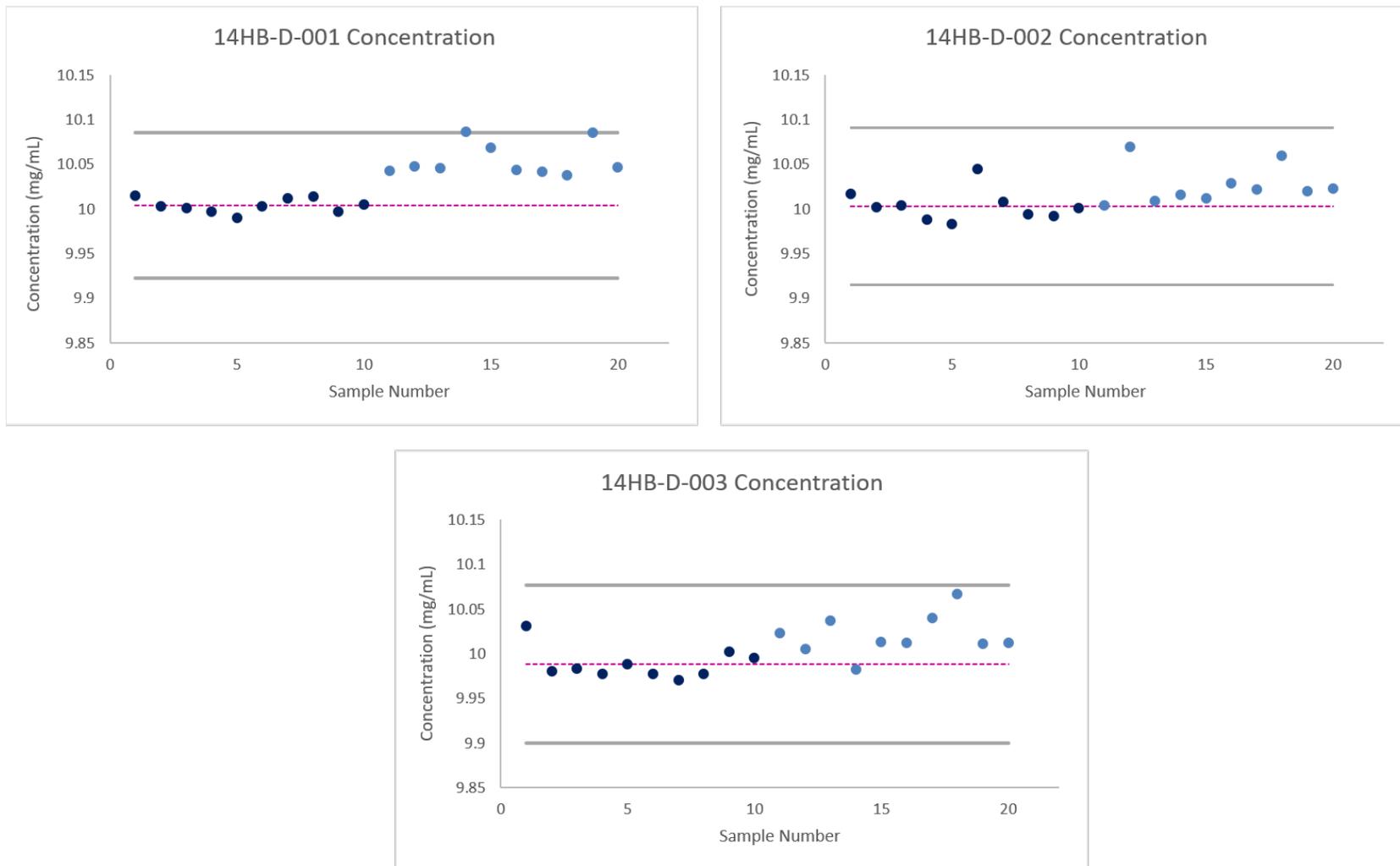
Figure 3. Mass concentration control chart using UV-Vis spectrophotometry.
Initial certification data is shown in dark blue and 5YSV data in light blue (Measured values listed in Appendix Table 1). Pink dotted line corresponds to the non-certified value assigned in the original 2016 certification. Control range set at ±2u_c (grey bars).

4.2. Size Exclusion Chromatography

4.2.1. Method

Size exclusion chromatography was utilized to confirm stability of the size heterogeneity of each RM 8671 lot.   The size heterogeneity and monomeric purity of NISTmAb RM 8671 were analyzed under non-denaturing conditions by SE-UHPLC with UV detection according to the qualified protocol [3, 5]. The only deviation to the previously reported protocol was with regard to data processing. Upon comparison of the 2016 and 5YSV chromatograms, it was determined that a small hump believed to be a baseline aberration was observed between the monomer and low molecular weight peaks (Figure 4). When the integration parameters from 2016 were applied to the most recent samples, the "hump" ($\approx$0.05% RA) was below the limit of detection (determined to be 0.135% in 2016) resulting in the software unable to identify it as a "true" peak [3]. As a result, the low molecular weight detection window limits required adjustment by manually moving the left bound to have it begin where the monomer detection windows ended. This adjustment expanded the peak window allowing for the hump to be detected as part of the low molecular weight species, consistent with the integration window from 2016.
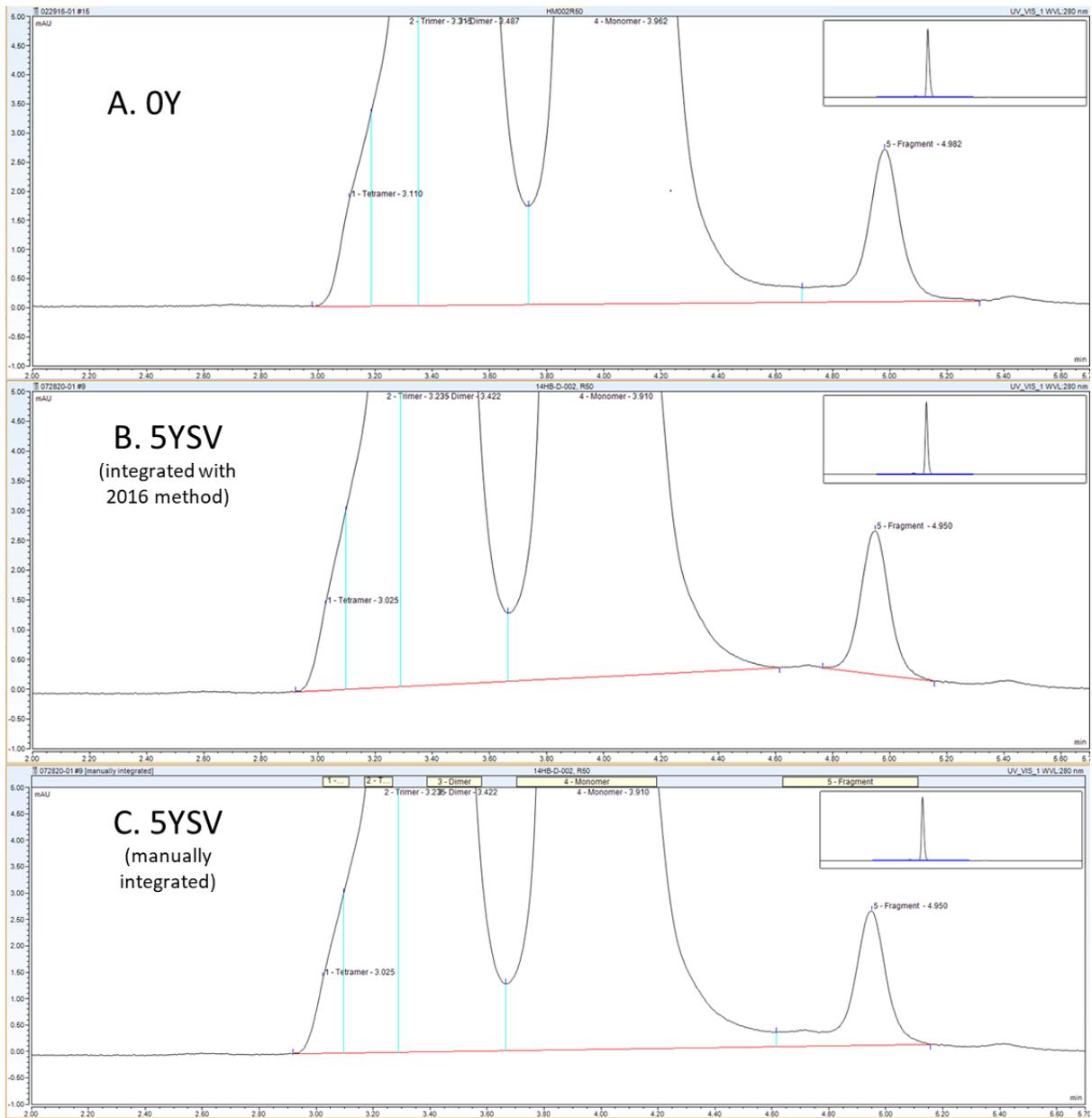
Figure 4. Comparison of integration parameters for SEC applied to 14HB-D-002.
(A) 2016 parameters applied to initial certification (0y) data, (B) 2016 parameters applied to 5YSV data, (C) manually integrated chromatogram for 5YSV.

4.2.2. Qualitative Results

A representative 5YSV chromatogram of 14HB-D-002 is shown in Figure 5 displaying the main species observed as high molecular weight (HMW), monomer, and lower molecular weight (LMW). The unlabeled peak at approximately 6.4 minutes was verified to be the void volume of the column and was due to elution of the L-histidine sample background buffer. The resultant chromatograms for all three RM 8671 lots were consistent in all salient features to that observed previously with the exception of the small baseline aberration below the limit of detection, evidenced by the fact that it is not visible in Figure 5. This aberration may simply be a manifestation of longitudinal method intermediate precision.
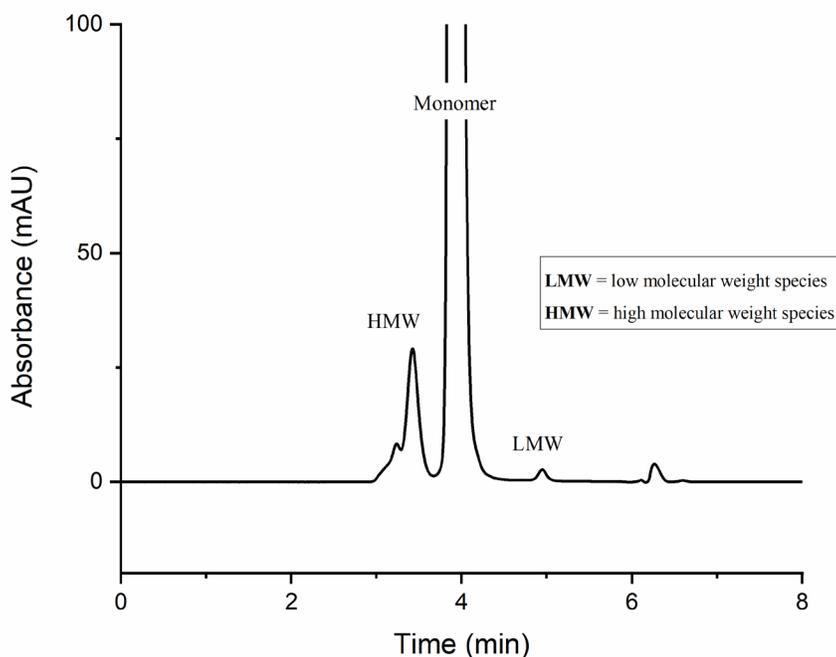
Figure 5. Representative chromatogram of RM 8671 Lot 14HB-D-002 by SEC.

4.2.3. Quantitative Results

The quantitative parameters considered for SEC stability analysis include monomeric purity (main peak) relative area (RA), high molecular weight (HMW) RA, and low molecular weight (LMW) RA. Results obtained during the stability assessment can be found in Table A2.

All PS 8670 system suitability runs conformed to expected performance criteria indicating the analytical measurement system was in control [6]. Control charts for RM 8671 are depicted in Figure 6, Figure 7, and Figure 8 for lots 14HB-D-001, 14HB-D-002, and 14HB-D-003 respectively. The control ranges were taken as the mean value ± three times the combined standard uncertainty ($\pm 3u_c$) determined in 2016[5]. All values for all lots are shown to be within the control range (grey bars) for each lot; the material is still homogeneous and stable with respect to size heterogeneity as determined by SEC, resulting in no change of the reference values or uncertainty.
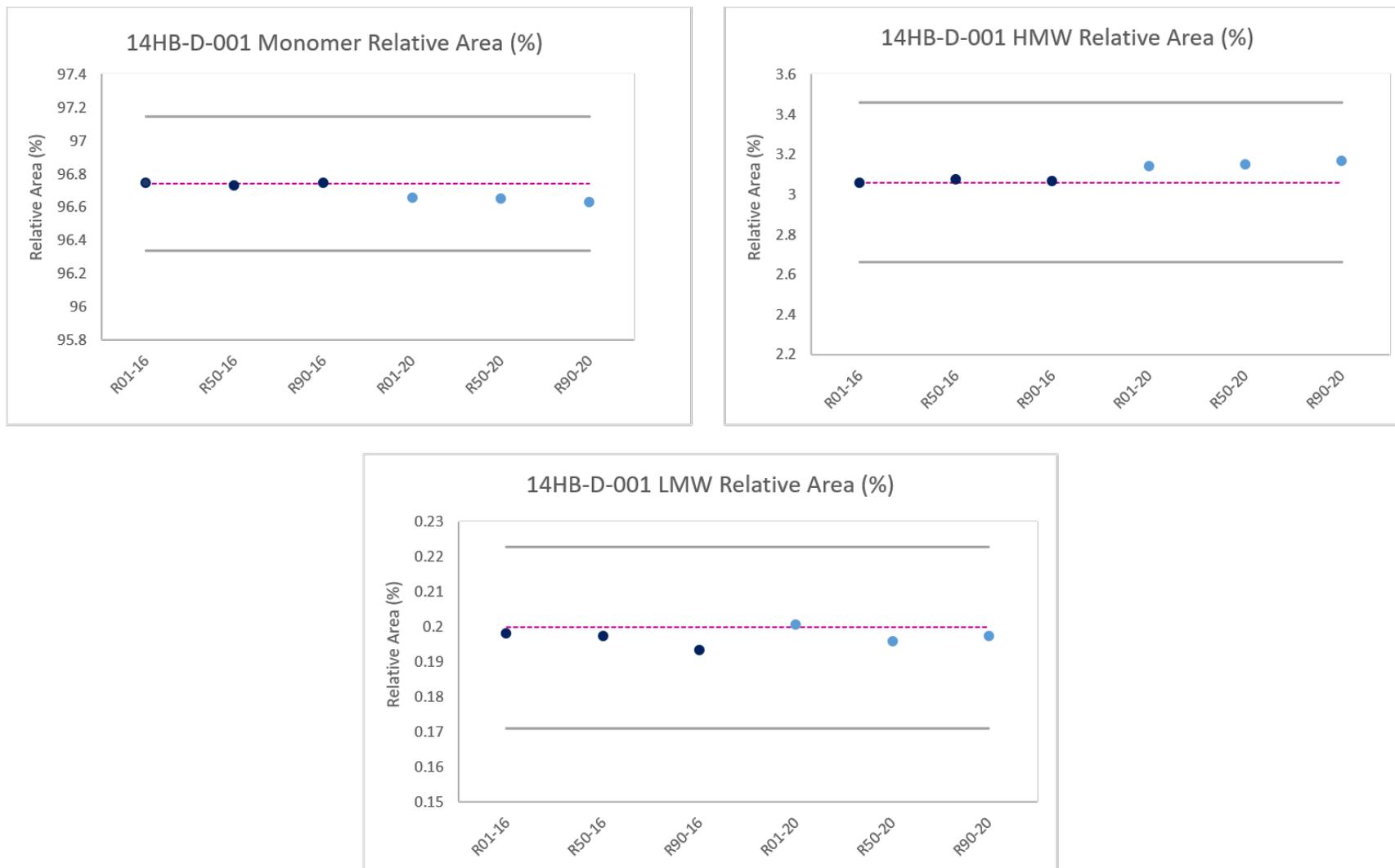
Figure 6. Size Heterogeneity control charts using size exclusion chromatography for lot 14HB-D-001.
Initial certification (0y) data is shown in dark blue and 5YSV (5y) in light blue. Pink dotted line corresponds to the non-certified value assigned in the original 2016 certification. Control limits set at ± 3u_c (grey bars)
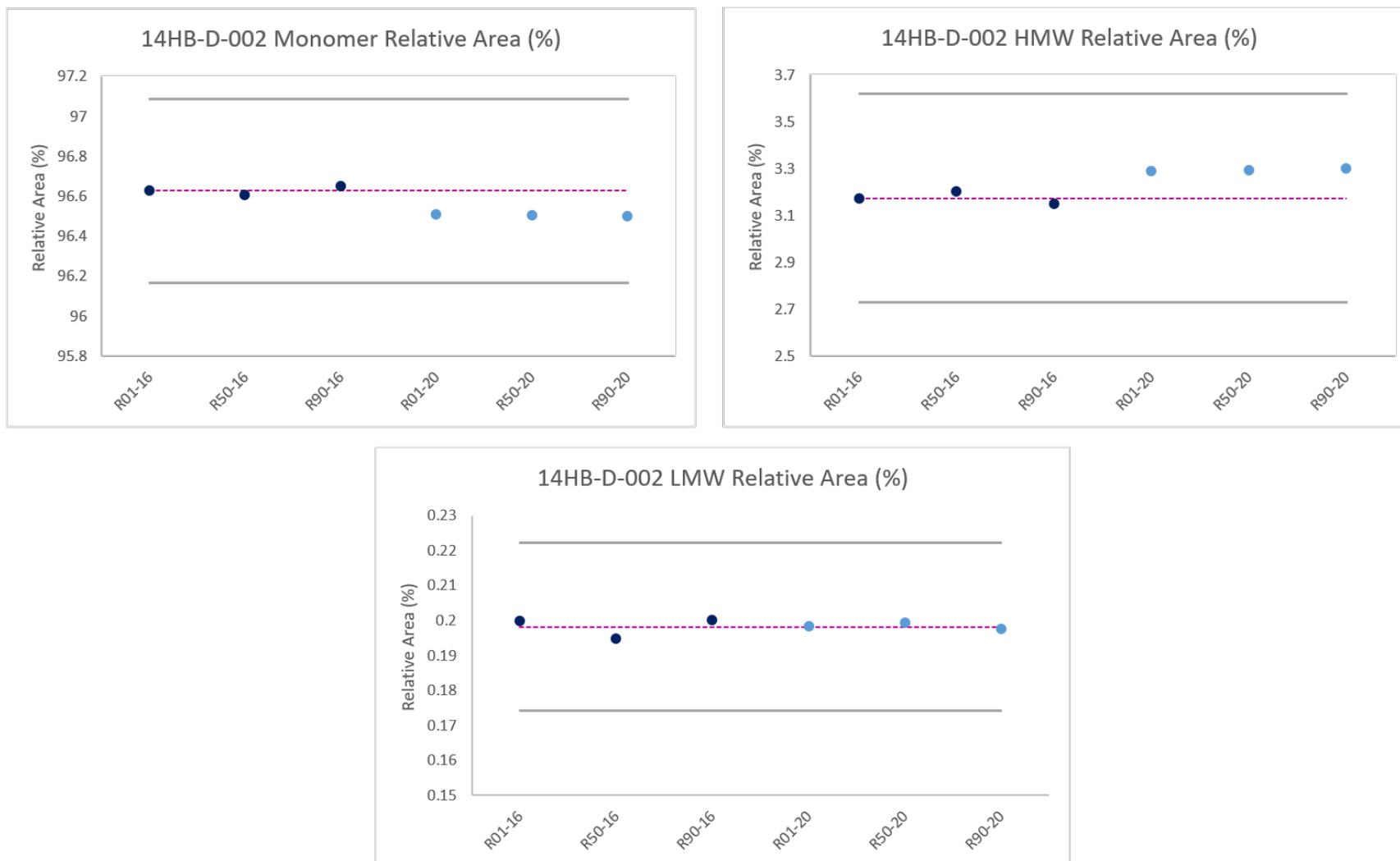
Figure 7. Size Heterogeneity control charts using size exclusion chromatography for lot 14HB-D-002.
Initial certification (0y) data is shown in dark blue and 5YSV (5y) in light blue. Pink dotted line corresponds to the non-certified value assigned in the original 2016 certification. Control limits set at ± $3u_c$ (grey bars)
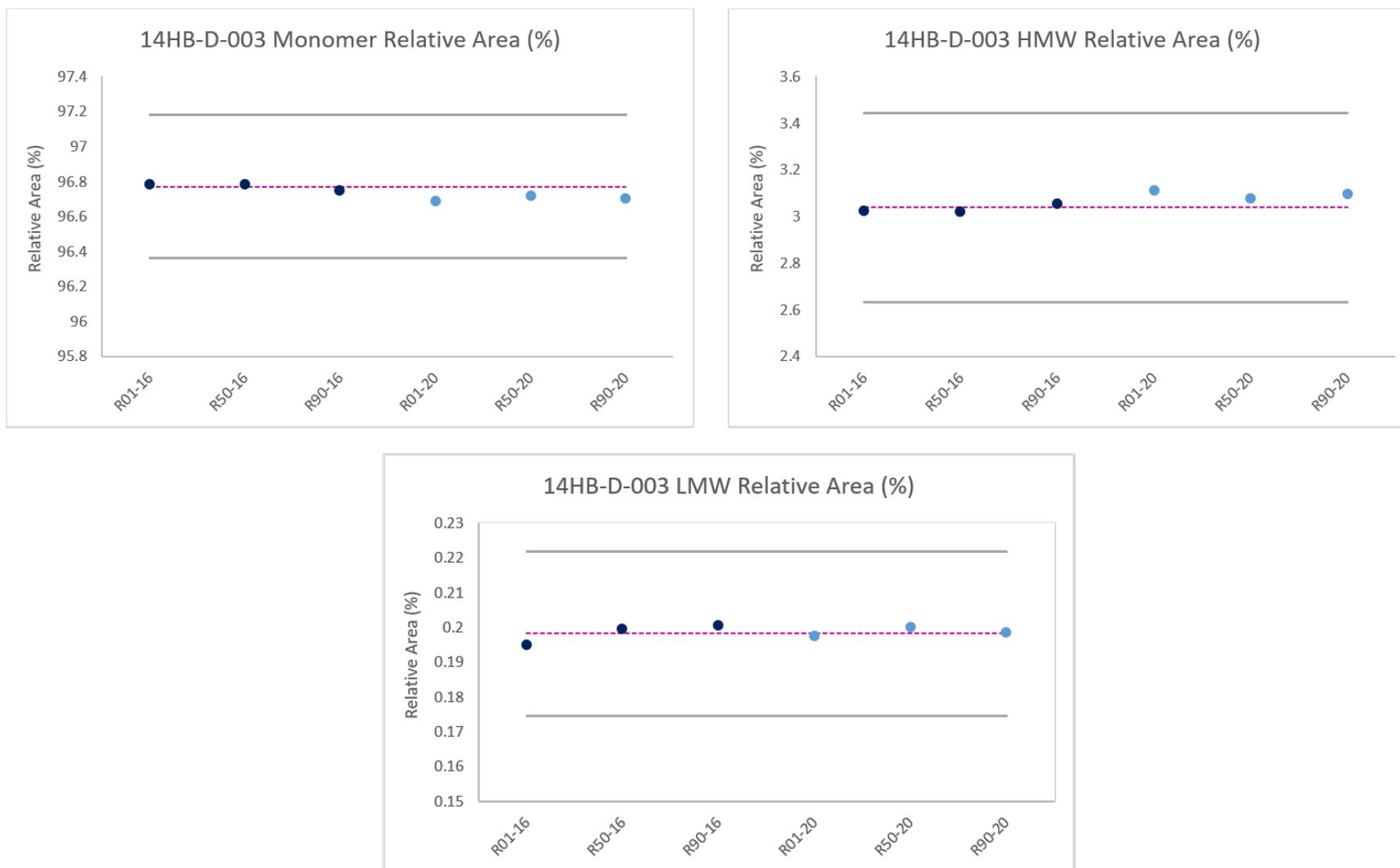
Figure 8. Size Heterogeneity control charts using size exclusion chromatography for lot 14HB-D-003.
Initial certification (0y) data is shown in dark blue and 5YSV (5y) in light blue. Pink dotted line corresponds to the non-certified value assigned in the original 2016 certification. Control limits set at ± $3u_c$ (grey bars)

4.3. Capillary Electrophoresis Sodium Dodecyl Sulfate

4.3.1. Method

Monoclonal antibody monomeric purity, glycan occupancy, and thioether content were quantified by capillary electrophoresis sodium dodecyl sulfate (CE-SDS). NISTmAb RM 8671 monomeric purity was measured by CE-SDS under non-reducing conditions (nrCE-SDS) according to the qualified method protocol. Non-reducing CE-SDS is employed to measure monomeric purity values; this is the abundance of the monomer relative to all mAb species detected. This method is sensitive to low molecular weight size variants (fragments) and to covalent aggregates. Non-covalent aggregates are disrupted during the sample preparation procedure, which involves denaturation in the presence of detergent. Glycan occupancies of the heavy chain and relative abundance of non-reducible species were measured by CE-SDS under reducing conditions (rCE-SDS) according to the qualified method protocol. The same PA 800 Plus instrument, software and CE-SDS MW analysis kit (Sciex PN: 390953) from original material certification were used [3]. The instrument was evaluated for its performance prior to analysis. The only exception to the previously reported protocol were the statistical considerations described in the statistical analysis section above.

4.3.2. Qualitative Results

A representative electropherogram of 14HB-D-002 under non-reducing conditions displaying the low abundance antibody fragments is shown in Figure 9 below. The resultant electropherograms for all three lots of RM 8671 were consistent in all salient features to that observed previously. Fragment peaks are observed at or below the limit of detection for the method which can affect the number of integrated peaks from injection to injection as shown in the electropherogram below.
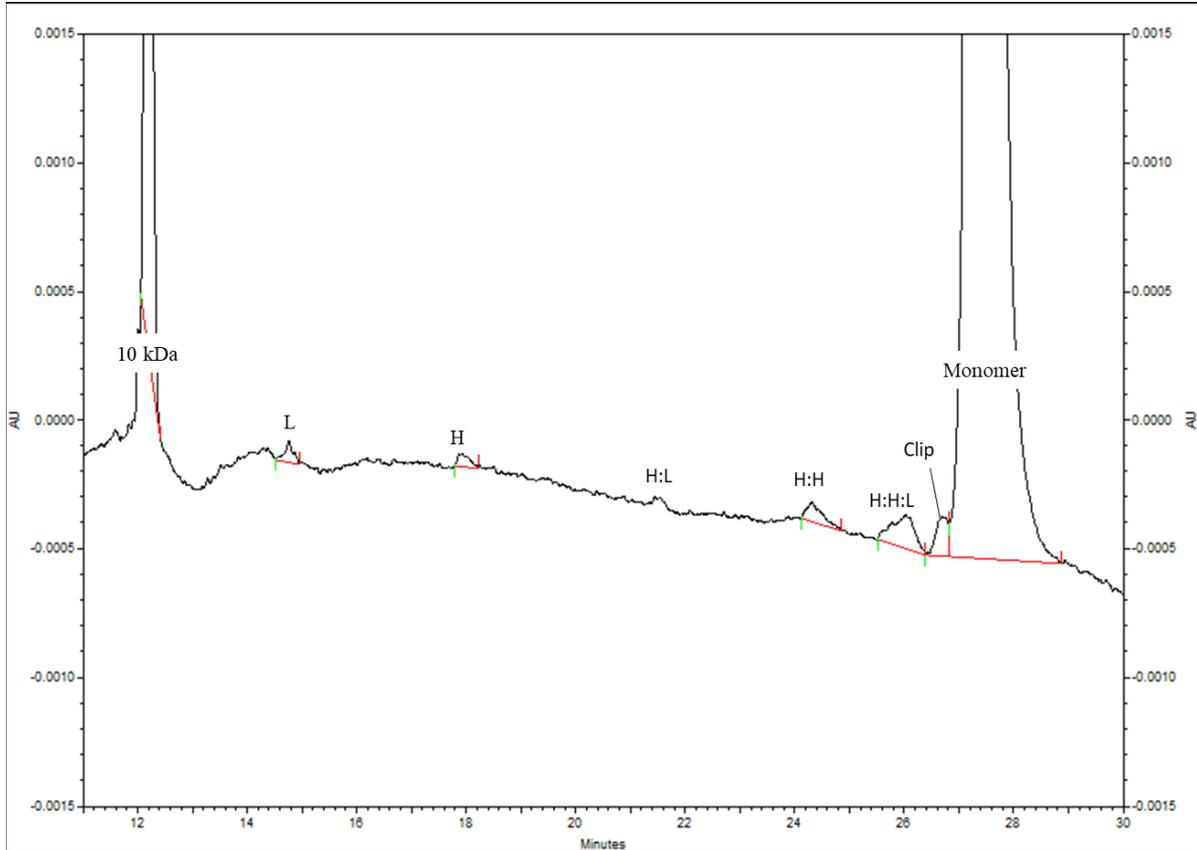
Figure 9. Representative electropherogram of 14HB-D-002 by CE-SDS under non-reducing conditions.
H: heavy chain; L: light chain; H:L : heavy-light half-antibody; H:H : heavy chain-heavy chain fragment; H:H:L : heavy chain-heavy chain-light chain fragment; clip: unidentified low molecular weight species; 10 kDa: internal standard.

A representative electropherogram of 14HB-D-002 under reducing conditions is shown in Figure 10 below. Four NISTmAb peaks are detected by reducing CE-SDS: light chain, aglycosylated/non-glycosylated heavy chain, heavy chain, and a non-reducible thioether-linked species (H:L thioether at heavy chain Cys223-light chain Cys213 verified via mass spectrometry peptide mapping). [7, 8] The resultant electropherograms for all lots of RM 8671 were consistent to all salient features observed previously.
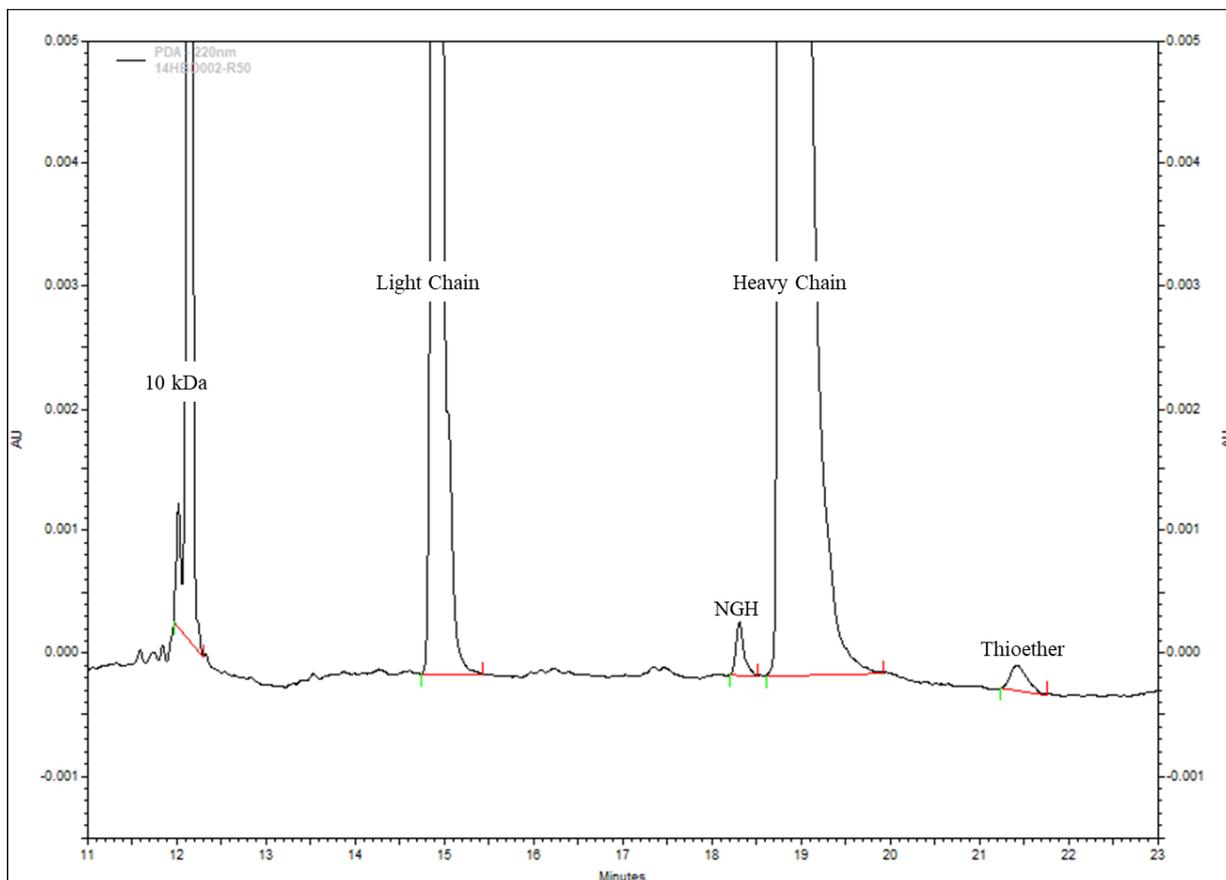
Figure 10. Representative electropherogram of 14HB-D-002 by CE-SDS under reducing conditions.
NGH: aglycosylated heavy chain

4.3.3. Quantitative Results

The quantitative parameters for CE-SDS (non-reduced and reduced) stability analysis include monomeric purity relative abundance (RA), glycan occupancy, and thioether relative abundance (RA). Results obtained during the stability assessment can be found in Table A3.

Control charts for each lot were prepared using the expanded uncertainty (u) calculated as three times the combined standard uncertainty (u_c) determined using equation 4 as detailed in the statistical analysis section above. Individual data points for each injection from 2016 and 5YSV are shown in Figure 11, Figure 12, and Figure 13 for lots 14HB-D-001, 14HB-D-002, and 14HB-D-003 respectively. All values are shown to be within the expanded uncertainty (grey bars) for each lot; the material is still homogeneous and stable. Stability measurements show that although there were minor shifts in performance due to inter-analyst variability, the material is still homogeneous and stable with regard to CE-SDS property values. The expanded uncertainty ranges now reflect true long-term intermediate precision contributions that were not factored in during initial certification (inter-user variability) which will be factored in to all future stability measurements.
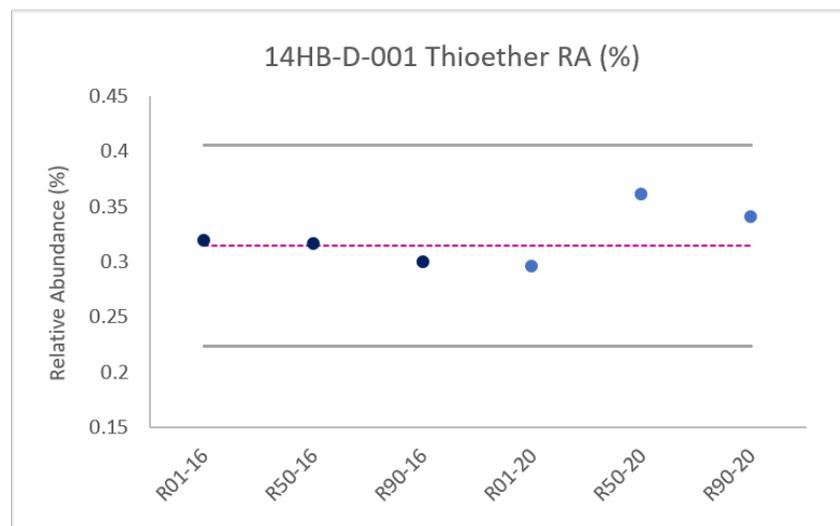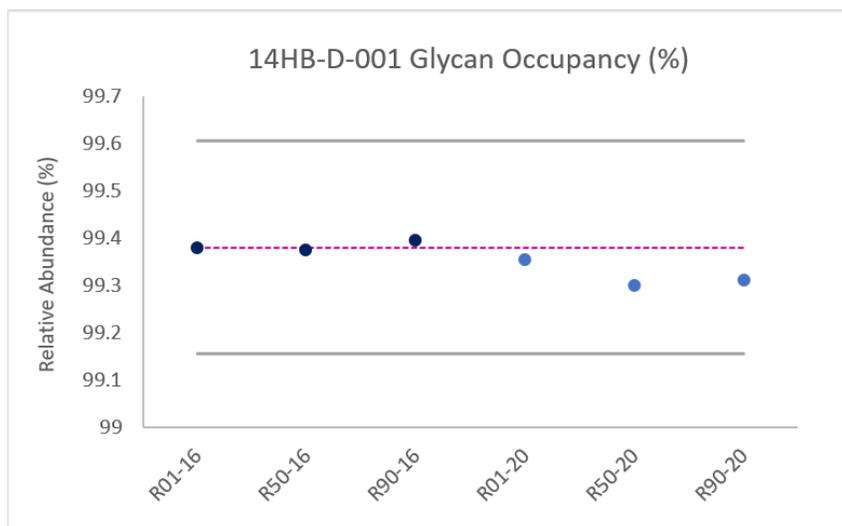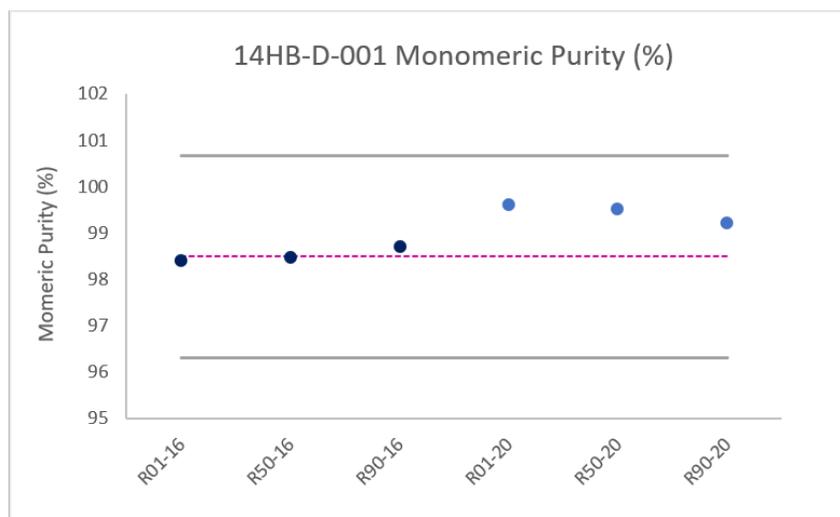
Figure 11. Size Heterogeneity control charts using capillary electrophoresis for lot 14HB-D-001.
Initial certification (0y) data is shown in dark blue and 5YSV (5y) in light blue. Pink dotted line corresponds to the non-certified value assigned in the original 2016 certification. Control limits set at ± $3u_c$ (grey bars)
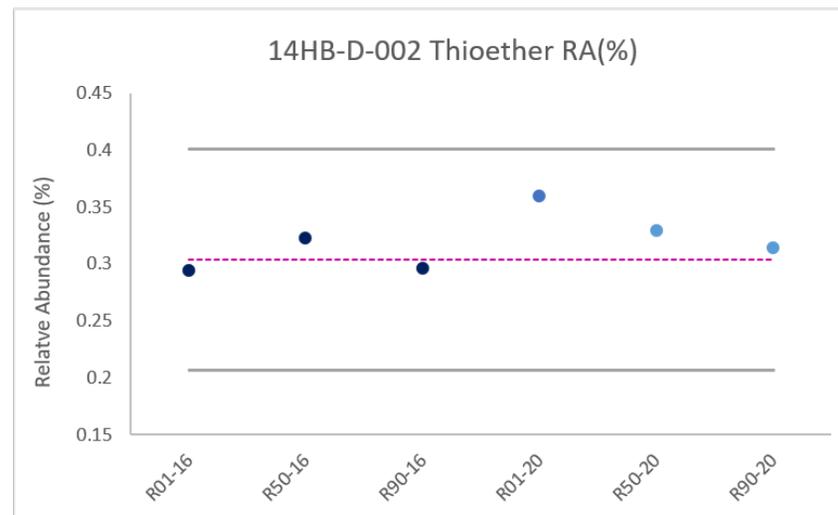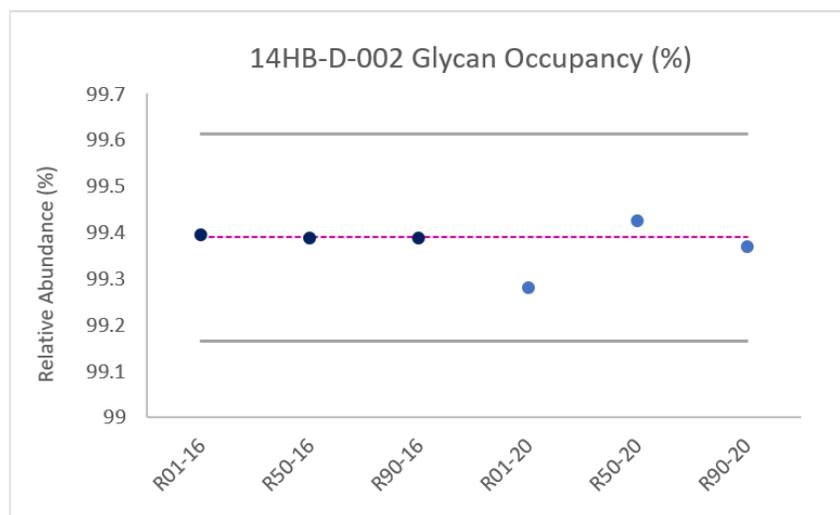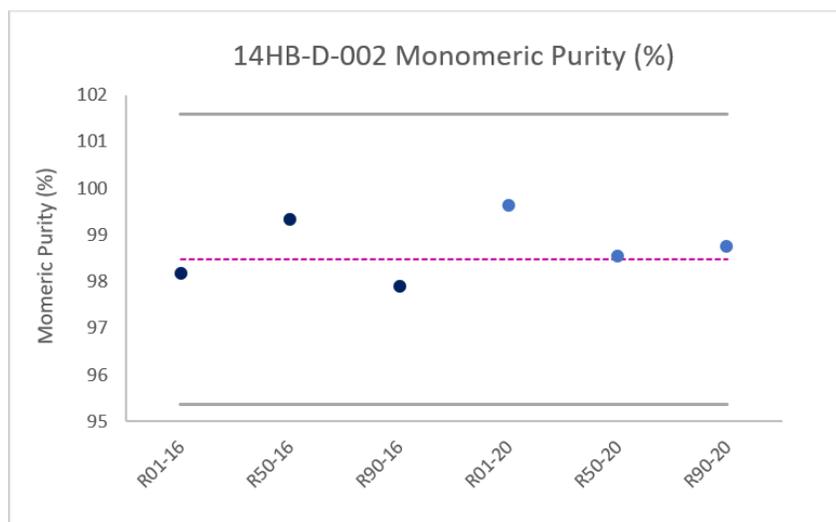
Figure 12. Size Heterogeneity control charts using capillary electrophoresis for lot 14HB-D-002.
Initial certification (0y) data is shown in dark blue and 5YSV (5y) in light blue. Pink dotted line corresponds to the non-certified value assigned in the original 2016 certification. Control limits set at ± $3u_c$ (grey bars)
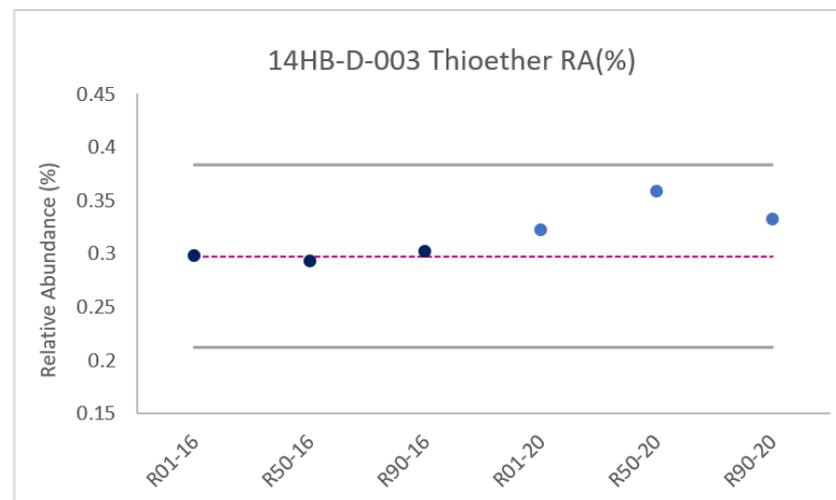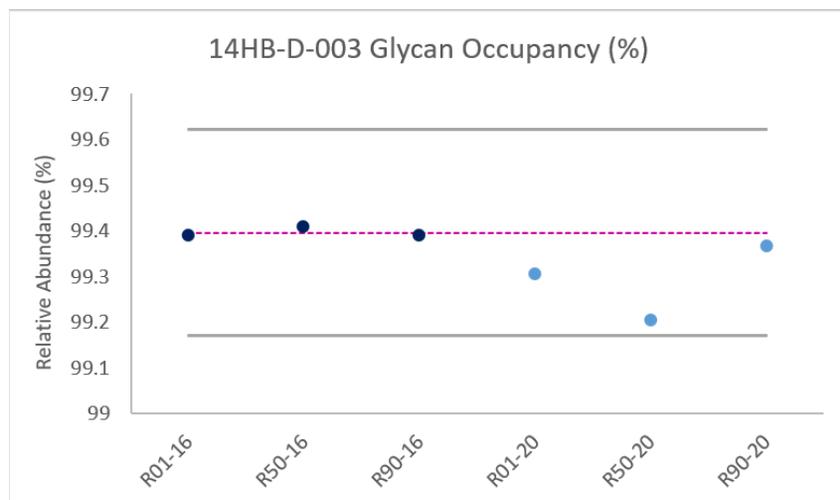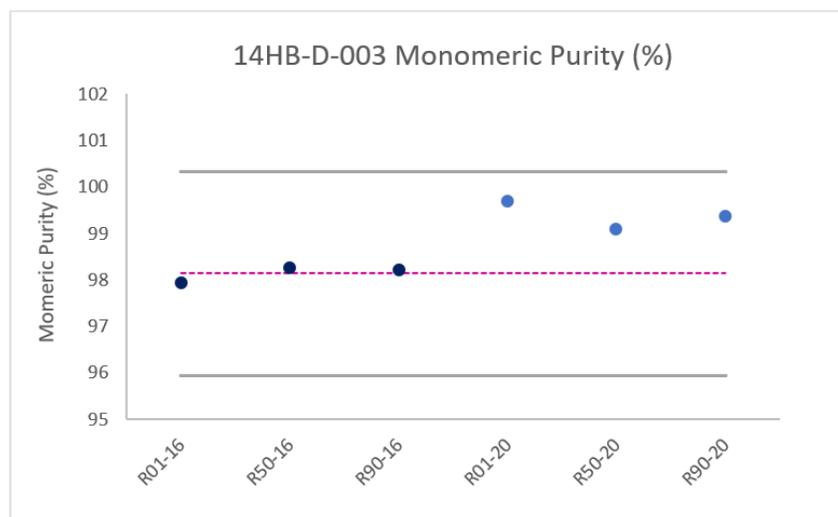
Figure 13. Size Heterogeneity control charts using capillary electrophoresis for lot 14HB-D-003.
Initial certification (0y) data is shown in dark blue and 5YSV (5y) in light blue. Pink dotted line corresponds to the non-certified value assigned in the original 2016 certification. Control limits set at $\pm\ 3u_c$ (grey bars)

4.4. Capillary Zone Electrophoresis

4.4.1. Method

NISTmAb charge heterogeneity was evaluated by the qualified CZE assay, wherein mAb charge variants are separated according to differential electrophoretic mobility in free solution within a uniform electric field applied across a buffer-filled fused silica capillary. The same PA 800 Plus instrument and software from original material certification were used [2]. The instrument was maintained and evaluated for its performance prior to analysis. The only exception to the previously reported protocol were the statistical considerations described above.

4.4.2. Qualitative Results

The CZE assay resolves the mAb sample into three charge groups: the main group, which comprises the majority of the sample; the basic variants, which migrate toward the cathode more rapidly than the main group; and the acidic variants, which migrate toward the cathode less rapidly than the main charge group as shown in Figure 14. The basic variants have previously been identified as C-terminal lysine variants with the C-terminal lysine present on either one (*) or both (**) heavy chain molecules[9]. The acidic variants co-migrate as a smear and comprise mAb presenting a variety of post-translational modifications (PTMs), including asparagine deamidation(s), lysine glycation(s), N-terminal glutamine, and sialic acid glycovariants. The charge purity of the NISTmAb is given as the relative abundance of the main charge group with respect to all detected charge species. A representative electropherogram of 14HB-D-002 is shown in Figure 14 below. The resultant electropherograms for all three lots of RM 8671 were consistent in all salient features to that observed previously.
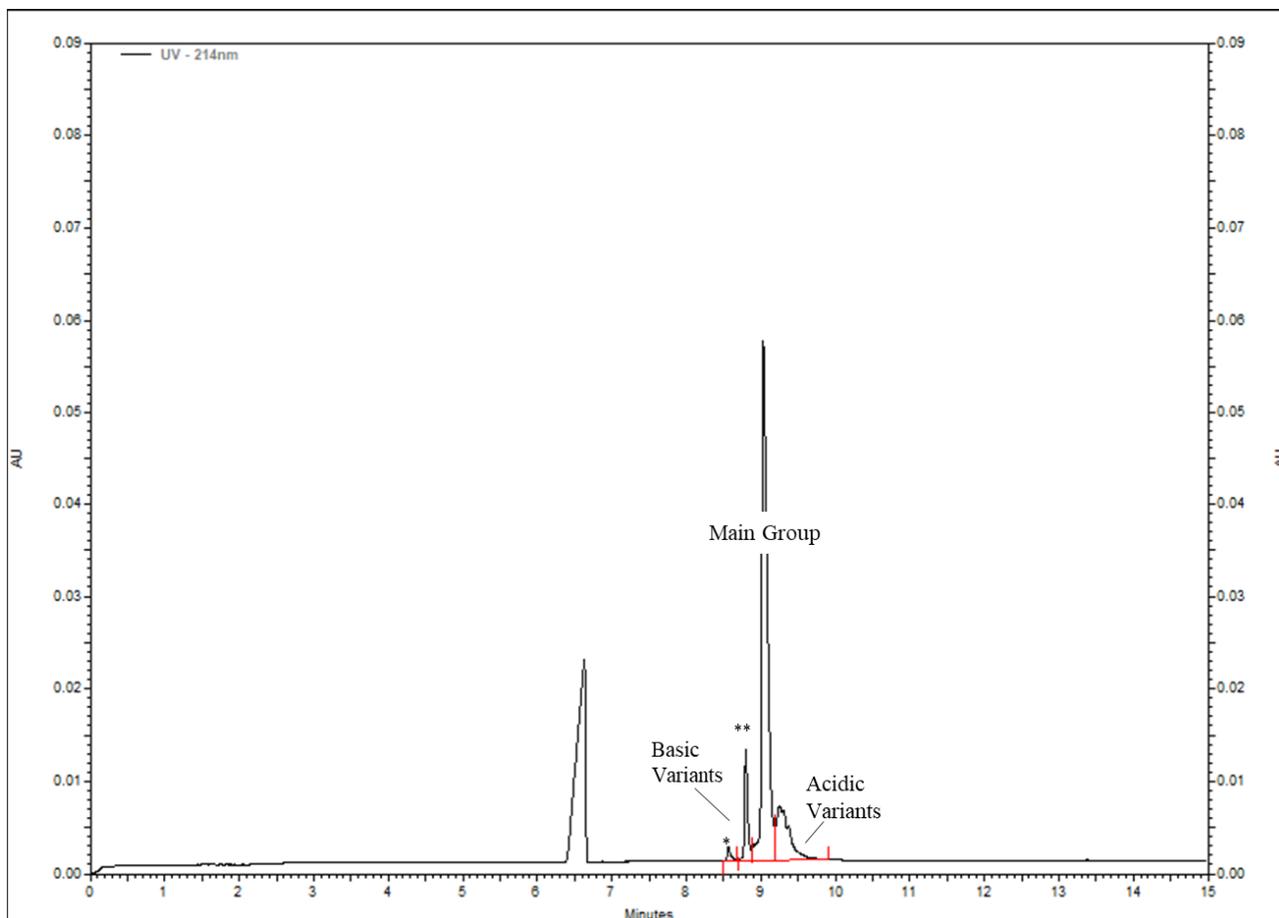
Figure 14. Representative electropherogram for lot 14HB-D-002 by CZE.
Baseline and integration limits are indicated by red horizontal and vertical lines, respectively. (*)
indicates 1K (1 des-lysine) peak. (**) indicates 2K (0 des-lysine) peak.

4.4.3. Quantitative Results

The quantitative parameters for CZE stability analysis include charge purity, basic variant relative abundance, and acidic variant relative abundance. Results obtained during the 5YSV stability assessment can be found in Table A4.

Control charts for each lot were prepared using the expanded uncertainty (U) calculated as three times the combined standard uncertainty (u_c) determined using equation 4as detailed in the statistical analysis section above. Individual data points for each injection from 2016 and 5YSV are shown in Figure 15, Figure 16 and Figure 17 for lots 14HB-D-001, 14HB-D-002, and 14HB-D-003 respectively. All values are shown to be within the expanded uncertainty (grey bars) for each lot; the material is still homogeneous and stable. All CZE stability results for all RM 8671 lots fall within the updated expanded uncertainty range. Stability measurements show that although there were minor shifts in performance due to inter-analyst variability the material is still homogeneous and stable with regard to CZE property values.

The expanded uncertainty ranges now reflect true long-term intermediate precision contributions that were not factored in during initial certification (inter-user variability) which will be factored in to all future stability measurements.
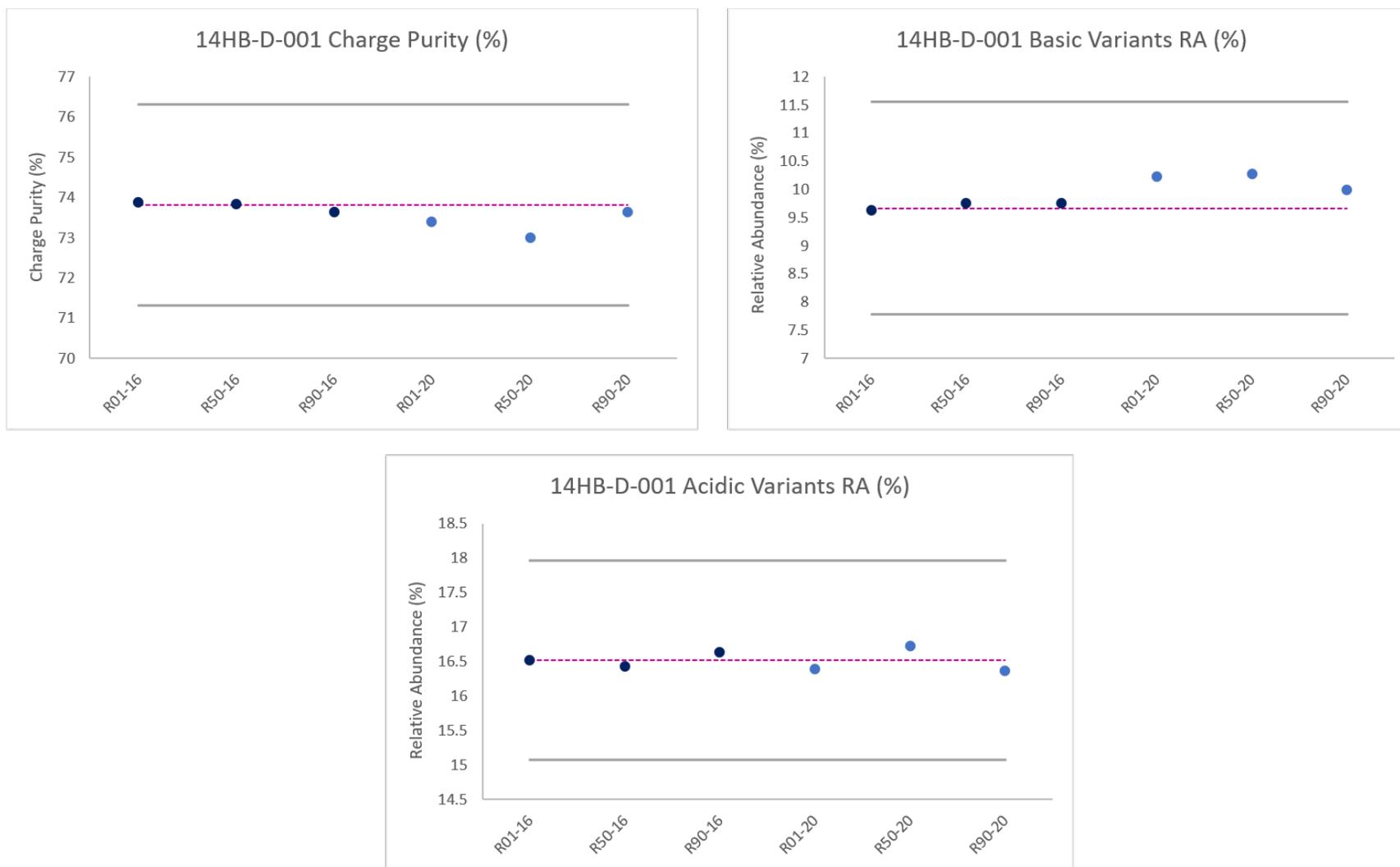
Figure 15. Charge heterogeneity control charts using capillary zone electrophoresis for lot 14HB-D-001.
Initial certification (0y) data is shown in dark blue and 5YSV (5y) in light blue. Pink dotted line corresponds to the non-certified value assigned in the original 2016 certification. Control limits set at $\pm 3u_c$ (grey bars)
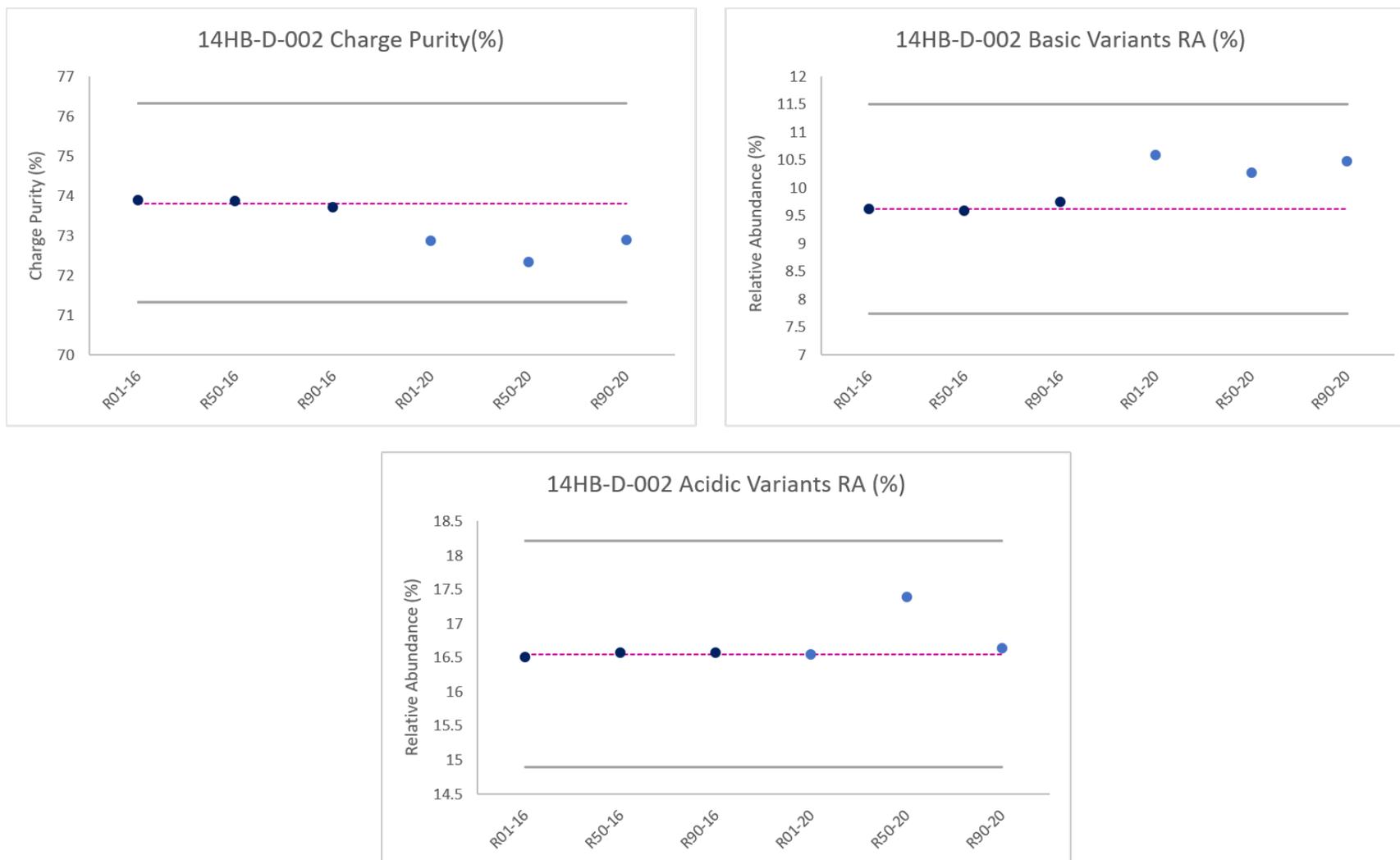
Figure 16. Charge heterogeneity control charts using capillary zone electrophoresis for lot 14HB-D-002.
Initial certification (0y) data is shown in dark blue and 5YSV (5y) in light blue. Pink dotted line corresponds to the non-certified value assigned in the original 2016 certification. Control limits set at $\pm\ 3u_c$ (grey bars)
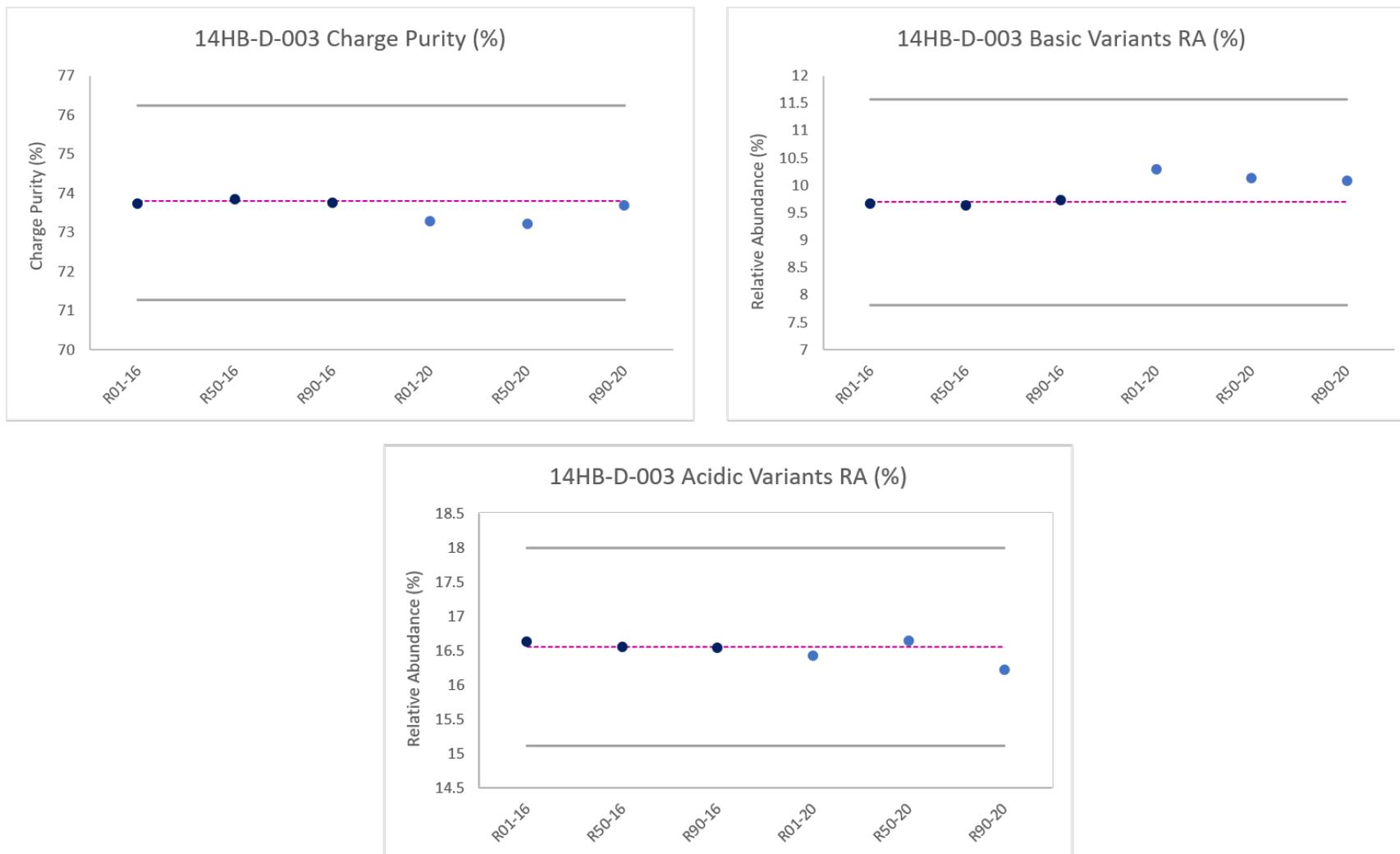
Figure 17. Charge heterogeneity control charts using capillary zone electrophoresis for lot 14HB-D-003.
Initial certification (0y) data is shown in dark blue and 5YSV (5y) in light blue. Pink dotted line corresponds to the non-certified value assigned in the original 2016 certification. Control limits set at ± $3u_c$ (grey bars).

4.5.   Dynamic Light Scattering

4.5.1. Method

Dynamic light scattering (DLS) is one of the methods used to assess the stability of each of the three RM 8671 lots. DLS measures the size distribution of particles ranging from 1 nm to 1 μm in size. Particles in a solution move randomly by Brownian motion and scatter light. By analyzing the fluctuations in the intensity of the scattered light as a function of time, the diffusion coefficient of the particles and consequently their size can be calculated.   The Z-average, or hydrodynamic, diameter of RM 8671 lots was evaluated according to the optimized protocol described previously [3, 5]. The only exception to the previously reported protocol is due to a software change that occurred since 2016. In 2016, Zetasizer software version 7.11 was used and in this report, the most recent 7.13 version was used. Along with RM 8671, 200 nm beads (Thermofisher, 3200A) and the Primary Sample 8670 material were run to assess the sizing accuracy of the instrument and for comparison to the earlier published values, respectively [3]. As before, the protein samples were measured directly without further dilution or any preparation steps. All samples were run in triplicates (from 3 vials), with each sample being acquired in 3 successive measurements, with 10 scans and with an equilibration time of 60 s ($n = 9$ total runs). The measurements were performed at 25˚C using a viscosity of 0.8872 mPa·s. The parameters measured was the Z-average hydrodynamic diameter. It was noted that for every run, the polydispersity index was below 0.2.

4.5.2. Qualitative Results

The current data fits the criteria that was previously observed for the NISTmAb. Representative intensity-based plots of the samples obtained in 5YSV are shown in Figure 18, with the peak centered around 10 nm, which is typical for monoclonal antibodies.   The presence of only the main peak shows that there is no observable aggregation in the 1 nm to 1000 nm size, or at least none detectable by this method.
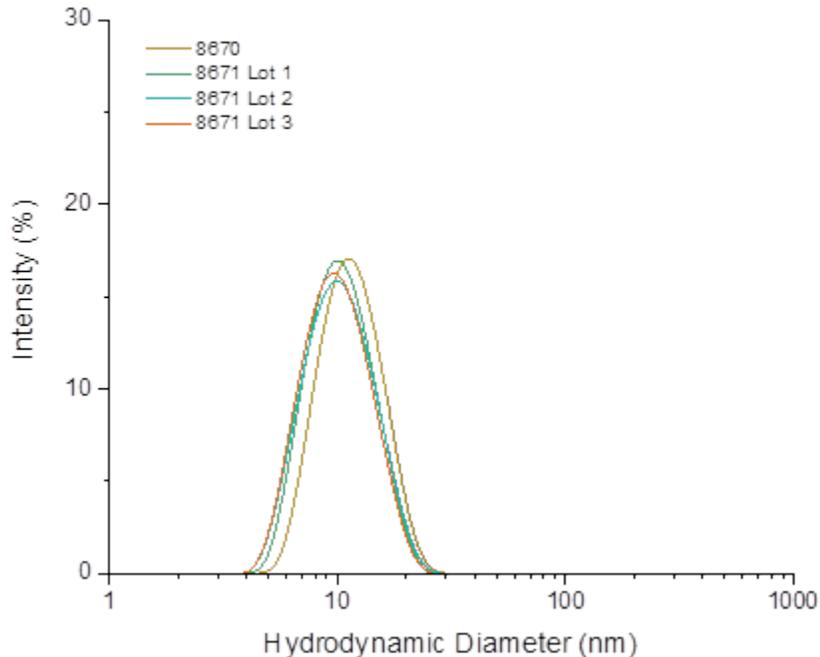
Figure 18. A representative intensity-based plot of Primary Sample 8670 and RM 8671 by DLS.

4.5.3. Quantitative Results

The quantitative parameter considered for DLS stability analysis is the Z-average hydrodynamic radius. Results obtained during the 5YSV stability assessment can be found in Table A5.

All PS 8670 system suitability runs conformed to expected performance criteria indicating the analytical measurement system was in control [3]. Control charts for each lot were prepared using the expanded uncertainty (U) calculated as three times the combined standard uncertainty (u_c) determined in 2016 [2]. Individual data points for each rack average from 2016 and 5YSV are shown in Figure 19 for lots 14HB-D-001, 14HB-D-002, and 14HB-D-003.
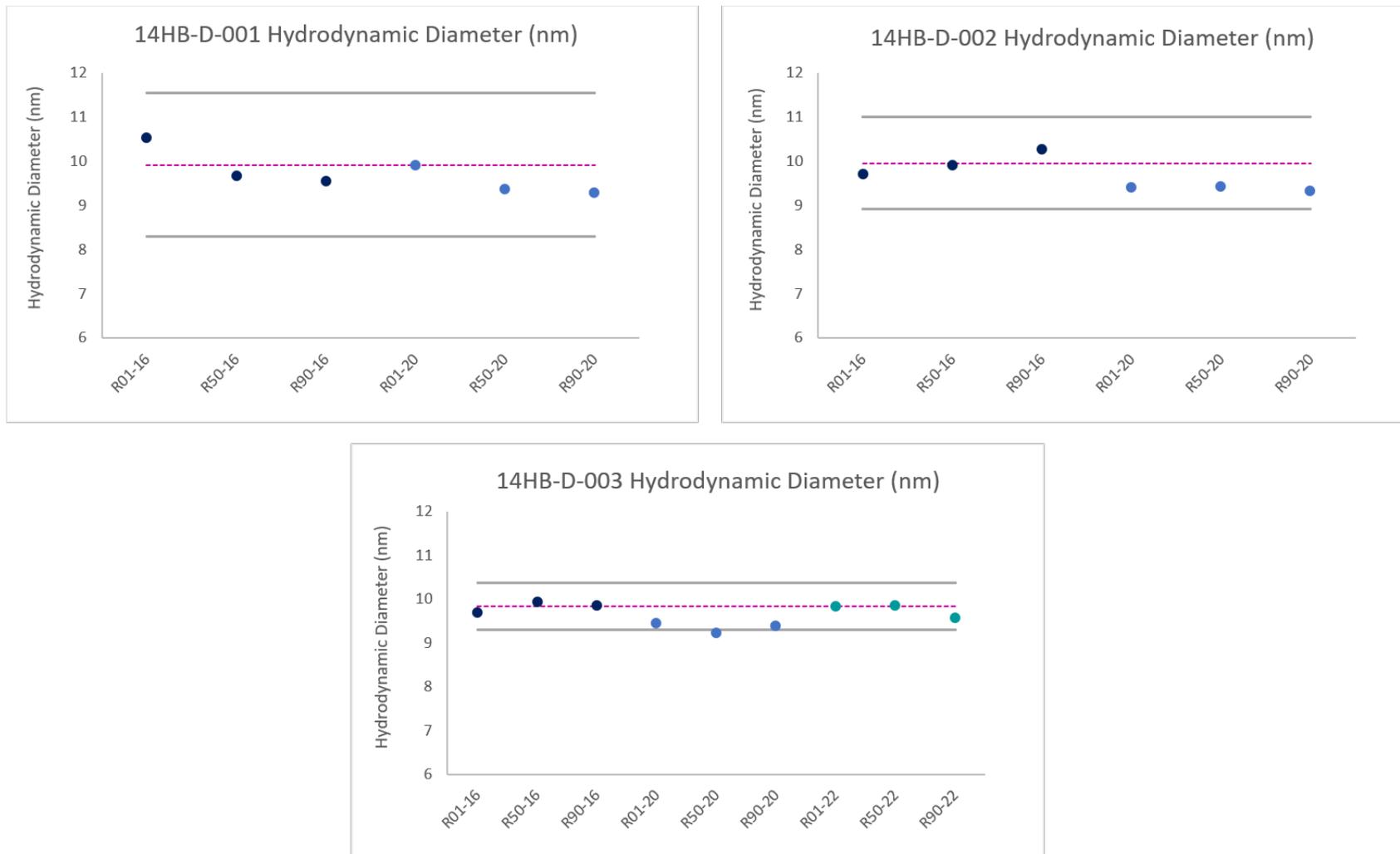
Figure 19. Average hydrodynamic diameter control charts using dynamic light scattering for lots 14HB-D-001, 14HB-D-002, and 14HB-D-003. Initial certification (0y) data is shown in dark blue, 5YSV 2020 (5yA) in light blue, 5YSV 2022 (5yB) in green. Pink dotted line corresponds to the non-certified value assigned in the original 2016 certification. Control limits set at ± 3u_c (grey bars)

As observed in Figure 19, the data scatter was consistent with 2016. A small apparent drift in global average was observed, albeit within the control limits of the method for lots 1 and 2. DLS is not a quantitative method so minor shifts such as these may be due to instrumental drift since the technique may not be able to pick up shifts in 1 to 2 nanometers. DLS stability results for lot 14HB-D-003 showed a minor shift, likely due to effect of long-term intermediate precision unaccounted for in the original uncertainty assessment performed over a relatively short period of time. The hydrodynamic diameter of 14HB-D-003 obtained in 2020 measured just outside the lower control limit for $k = 3$. It was determined that lot 3 would be remeasured to check if this observation truly indicates that the hydrodynamic diameter is measuring outside of the lower control limit or if it is just due to the low number of samples being analyzed (n =3 vials). Three new vials from lot 3 were remeasured using identical parameters as those used in earlier measurements. The only difference is that in 2022, 3 aliquots were taken from each of the 3 vials and measured.

Contributions due to temperature drift were ruled out based on consistent agreement of the nanometer sizing beads (Table A5). Slight changes in the material itself also seem unlikely as both orthogonal size methods (SEC and CE-SDS) showed no changes in the fragmentation or aggregation of the material. It is therefore likely that this small apparent shift is likely a result of long-term intermediate precision due to instrumental drift, aging of the instrument, or automatic software change.   The latest measurements, obtained in 2022, fall within the upper and lower control limits for this lot.

DLS stability results for RM 8671 lots 14HB-D-001 and 14HB-D-002 fall within the expanded uncertainty range assigned during the original value assignment in 2016. Lot 14HB-D-003 showed a minor shift in hydrodynamic radius, likely a result of long-term instrumental drift, aging of the instrument, or automatic software change. Stability measurements therefore show that the material is still homogeneous and stable with regard to DLS property values

5. Additional Characterization Methods

5.1.   Flow Imaging

5.1.1. Method

Flow Imaging is one of the methods used to assess the stability of each of the three RM 8671 lots. The technique is used to measure the size distribution of subvisible particles ranging from 2 μm to 100 μm in size (referred to as $N (\geq 2$ μm), or the cumulative particle concentration above 2 μm). Bright-field images of the particles are captured in successive frames as a stream of sample passes through a flow cell positioned in the field of view of a microscopic system. The captured digital images of the particles present in the sample are stored in a database that can be retrieved and analyzed for size, count, transparency, and many other morphological parameters.

The subvisible particle content in the three lots of RM 8671 were evaluated according to the optimized protocol described previously [3, 5]. The same flow imaging instrument and software were used to capture the data; the instrument was evaluated for its performance and calibrated as described previously. The only exception to the previously reported protocol is that the Lumetics software and the Python script were not used to calculate the mass of protein within protein particles. Instead, the final particle concentrations were obtained solely through the flow imaging acquisition software (MVSS V.2, Protein Simple, San Jose, CA) and the analysis software (MVAS 1.4, Protein Simple, San Jose, CA). A subset of the data was analyzed by the flow imaging instrument data software and the Python script; there were no differences in the results obtained by either method (data not shown).

The flow cell used in 2016 was replaced with a new, similar silane coated flow cell (serial # 0122202) from Protein Simple. Along with RM 8671, 5 µm Count-Cal beads of nominal 3000 mL^{-1} concentration (Lot: 232956, Thermo Scientific, Waltham, MA) and the Primary Sample (PS) 8670 material were run to assess the sizing and counting accuracy of the instrument and for comparison to the earlier published values, respectively [3]. The particle concentrations obtained with the Count-Cal beads were lower than the manufacturer's specifications; this suggested that the flow cell was slightly smaller than expected. To determine the deviation of the flow-cell thickness from the manufacturer's reported 100 µm thickness, a primary bead standard, consisting of 4 µm polystyrene beads, was analyzed on the flow imaging and light obscuration methods. On both methods, we found the concentration difference between 2 µm and 8 µm, labeled (2-8) µm. We applied a coincidence error to the (2 to 8) µm concentration obtained by light obscuration by multiplying the value by 1.0495 [10]. A ratio of the corrected light obscuration concentration to the flow imaging concentration for the (2 to 8) µm size range gives the correction factor. The correction factor was determined to be 1.13. This means that the light obscuration was over-counting the 4 µm beads by 13% compared to the flow imaging system. This correction factor was applied to all of the raw concentration data in this report to adjust for the smaller-than-expected flow-cell of the flow imaging system.

As before, the protein samples were measured directly without further dilution. The sample requirements for flow imaging are high, so multiple runs could not be made from the same vial, i.e. each vial provided material for only 1 run. Therefore, all samples were run from multiple vials (5 to 6 vials), with 0.7 mL being loaded, 0.2 mL being purged, and 2 mL of water being run between samples. The optimization step was performed with particle free water. All sample runs, before being included in the analysis, were inspected for air bubbles that were larger than 10 µm and filters were applied appropriately to correct for them.

5.1.2. Results

The quantitative parameter considered for stability analysis is the number concentration of subvisible particles above 2 µm (labeled $N(\geq 2$ µm)). Results obtained during the 5YSV can be found in Table A6.

All PS 8670 system suitability runs conformed to expected performance criteria indicating the analytical measurement system was in control. Control charts for each lot were prepared

using the expanded uncertainty (U) calculated as three times the combined standard uncertainty (u_c)[5]. Individual data points for each rack from 2016 and 5YSV are shown in Figure 20 for lots 14HB-D-001, 14HB-D-002, and 14HB-D-003. Each rack, within each lot, was analyzed in two runs (n = 1 and n = 2). The only exception is that for D-001, where rack 90 was only analyzed once in 2016. As observed in Figure 20, the extent of data scatter observed in 5YSV is consistent with what was observed in 2016. The three lots are consistent with one another in terms of total particle content ≥ 2 μm (within $\pm$ 3 SD). Stability measurements therefore show that these three lots are still homogeneous and stable with regards to subvisible particle concentration values.
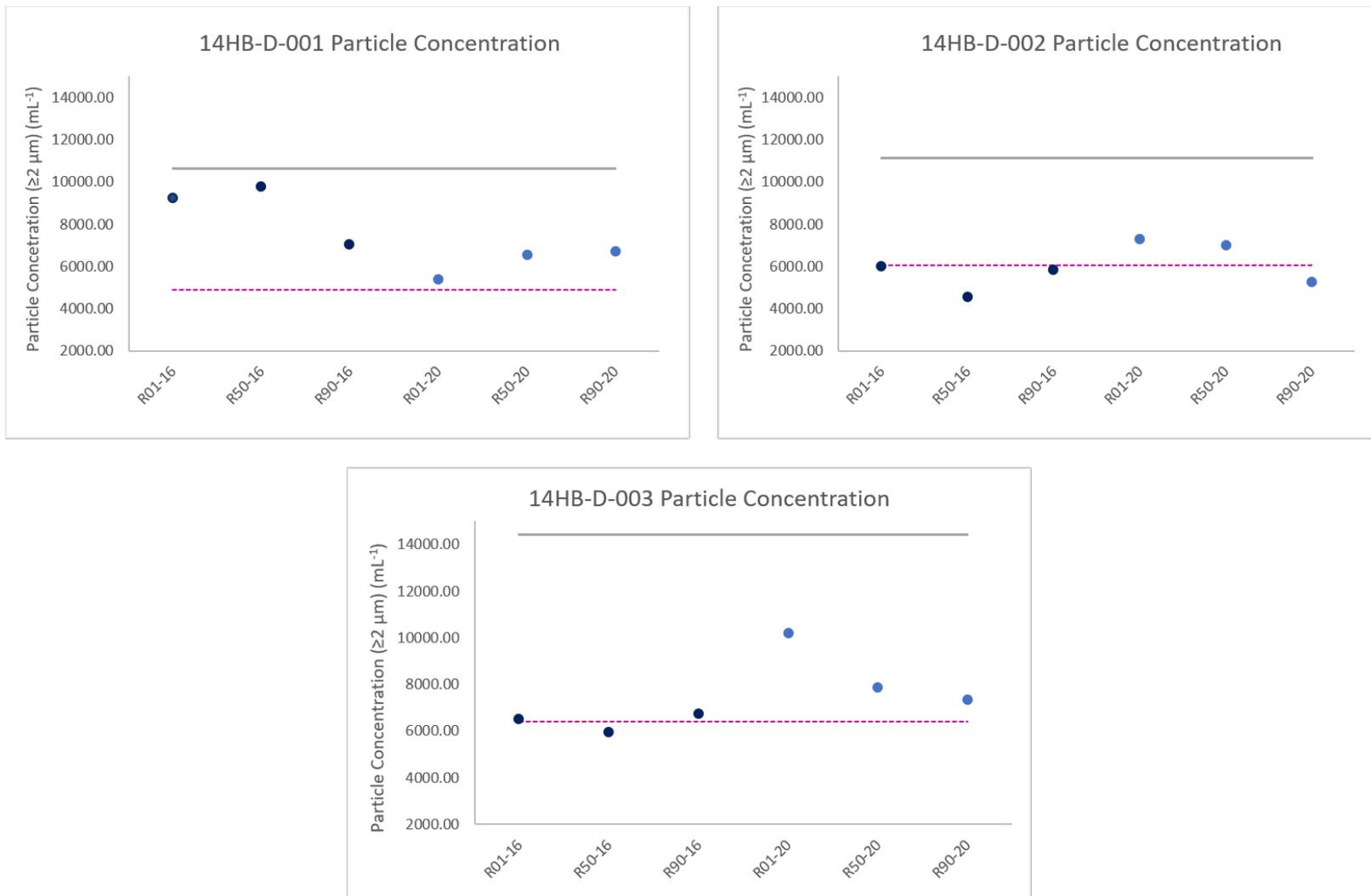
Figure 20. Particle concentration (N ≥ 2 µm) using flow imaging for lots 14HB-D-001, 14HB-D-002, and 14HB-D-003. Initial certification (0y) data is shown in dark blue and 5YSV (5y) in light blue. Pink dotted line corresponds to the non-certified value assigned in the original 2016 certification. Control limits set at ± $3u_c$ (grey bar). Only the upper control limit was taken as the mean value of the unstressed A) 14HB-D-001 + 3 SD B) 14HB-D-002 + 3 SD or C) 14HB-D-003 + 3 SD. (n = 2 for each rack).

5.2.   Peptide Mapping

5.2.1. Method

Qualitative peptide mapping was performed using ultrahigh-performance liquid chromatography (LC) coupled with online ultraviolet (UV) and tandem mass spectrometry [11] detection (LC-UV-MS/MS) to evaluate the primary structure of PS 8670 and confirm its identity to the RM lots. Peptides produced via the enzymatic digestion of a reduced and alkylated protein are resolved using LC-UV-MS/MS. A chromatographic trace, or peptide map, results from the signal generated as peptides eluting from the LC column pass through the UV and MS detectors ("peaks"). Differing amino acid sequences and post-translational modifications give each peptide unique chromatographic properties, such that even small differences at the peptide level easily translate into discernible differences in the landscape of the map. Differences between two protein molecules are likely to be observed when comparing their peptide maps due to differences in their chromatographic profiles.

MS instrumentation was used here in addition to UV detection not only to generate a visual peptide map, but also as a means of confirming the identity and amino acid sequence of the analytes. Both the accurate mass of intact peptides detected by MS as well as data generated through tandem MS ("MS/MS") analysis are used here for this purpose.

Peptide mapping of PS 8670 and the RM lots were performed using the same instrumentation (Thermo Orbitrap Discovery coupled to Dionex UltiMate 3000 LC system) and sample preparation method (tryptic digestion) as were used for the original certification of the material with a few exceptions made to improve the reproducibility of the method or due to discontinuation of reagents[12]:

1) EDTA was replaced with Sigma-Aldrich catalog #431788
2) DTT was replaced with Thermo Scientific Pierce catalog #A39255 (this is presumably the same product as previously used, but catalog number was changed by manufacturer due to change in packaging)
3) the protein was denatured at 3 µg/µL in denaturing buffer comprising 8 mol/L guanidine HCl, 1.3 mmol/L EDTA in 0.13 mol/L Tris, pH 7.8
4) the protein was reduced with 15 mmol/L dithiothreitol and alkylated with 28.8 mmol/L iodoacetamide
5) digestion was performed in buffer comprising 1 mol/L urea, 0.13 mol/l Tris, pH 7.8 with a trypsin:IgG ratio of 1:18
6) after buffer exchange, protein concentrations were measured and samples diluted to 0.5 µg/µL with digestion buffer; after digestion samples were diluted to 0.25 µg/µL with 0.1 % formic acid
7) Mobile solvents for LC analysis were replaced with Honeywell #14281-2L (0.1 % formic acid in water) and Honeywell # 34668-2.5L (0.1 % formic acid in acetonitrile)
8) sample injections were bracketed with injection of 20 pmol of a retention time standard (Thermo Scientific #88321, diluted to 0.5 pmol/µL with 0.1 % formic acid)
9) sample injections were made in duplicate, one each in MS-only mode and one in MS/MS mode

5.2.2. Results

The 5YSV peptide map generated from PS 8670 resulted in a chromatographic profile that differed from the original 2016 certification (Figure 21 and Appendix Figure A1, Figure A2 and Table A1). Likely causes for these differences are the change in solvent manufacturer for the mobile phase and the use of a new column lot. New and missing peaks were reviewed and determined to be the result of variations made to the digestion method or to the changes in chromatography (e.g. a low-abundant species that previously co-eluted with an abundant peptide was included as a trace-level component of a TIC peak in the original data set, but in the current set it is resolved from the abundant peptide and is not abundant enough by itself to meet the TIC peak threshold). The current peptide map resulted in slightly lower sequence coverage (heavy chain 96 %, light chain 99 %, Figure 21) as compared to the original map (heavy chain 97 %), light chain 100 %) due to lack of detection of 2- to 4-mer peptides whose signal was likely suppressed by co-eluting buffer components that were not present in the original map. Appendix Figure A1 and Table A1 provide a comprehensive comparison between the peptide maps.

A parallel sample preparation of 5YSV PS 8670 was directly compared to the 5YSV RM 8671 lots with respect to visual appearance and peak retention times of the total ion chromatogram (TIC) and the UV peptide map at 214 nm. Qualitative comparison showed consistent chromatographic profiles with no new or missing peaks between the samples (Figure 21), indicating their high level of sameness. Collision induced dissociation MS/MS peak identifications corresponding to peptides derived from the putative NISTmAb sequence were used to confirm identity and assure RM 8671 lot conformance with the PS. PS 8670 and each lot of RM 8671 demonstrated identification of the same peptides in the 5YSV analysis, therefore RM 8671 conformed to the identity of PS 8670.

Although there were changes observed in the peptide map over time, it appears these differences are predominantly a result of unavoidable changes in the sample preparation and analytical method rather than a change to the material. This hypothesis is supported by the fact that the primary structure of PS 8670 and the three RM lots conform to one another in the current 5YSV data. More importantly, each of the prior physicochemical methods indicate that the material is stable and homogeneous. The identity of each RM 8671 lot was found to conform to that of PS 8670.

A)
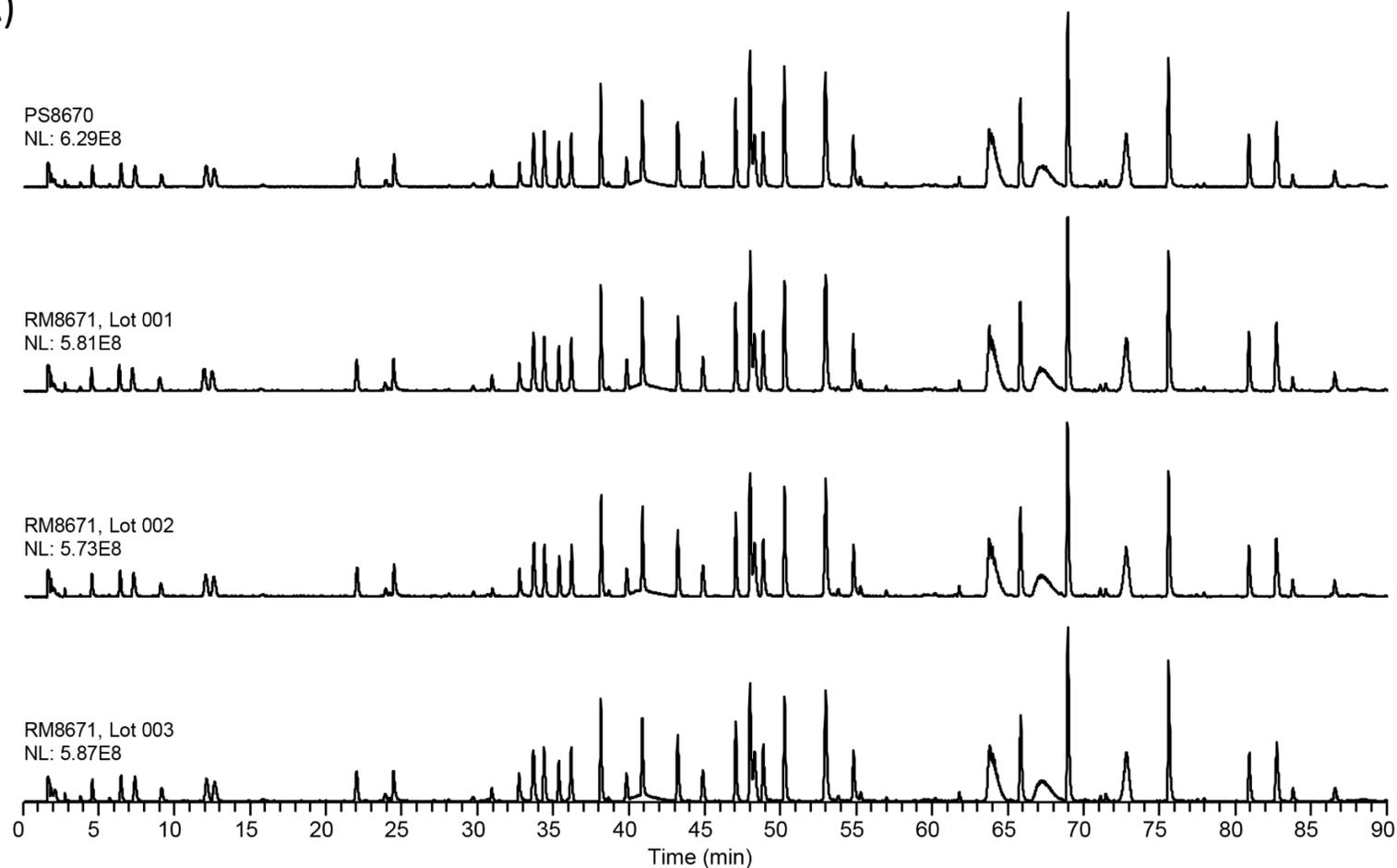
Figure 21. Alignment of 5YSV PS 8670 peptide map with 5YSV chromatograms lots 14HB-D-001, 14HB-D-002, and 14HB-D-003. Tryptic digests of the three RM lots were analyzed by LC-UV-MS and the similarity of the resulting A) TIC and B) UV chromatograms compared against the reference peptide map generated from the PS8670 digest as depicted in the top trace of each panel. The initial five minutes of the UV traces are not shown due to the large difference in scale between the relative levels of absorbance during peaks detected during the 0 min to 5 min period and the 5 min to 90 min period.

B)
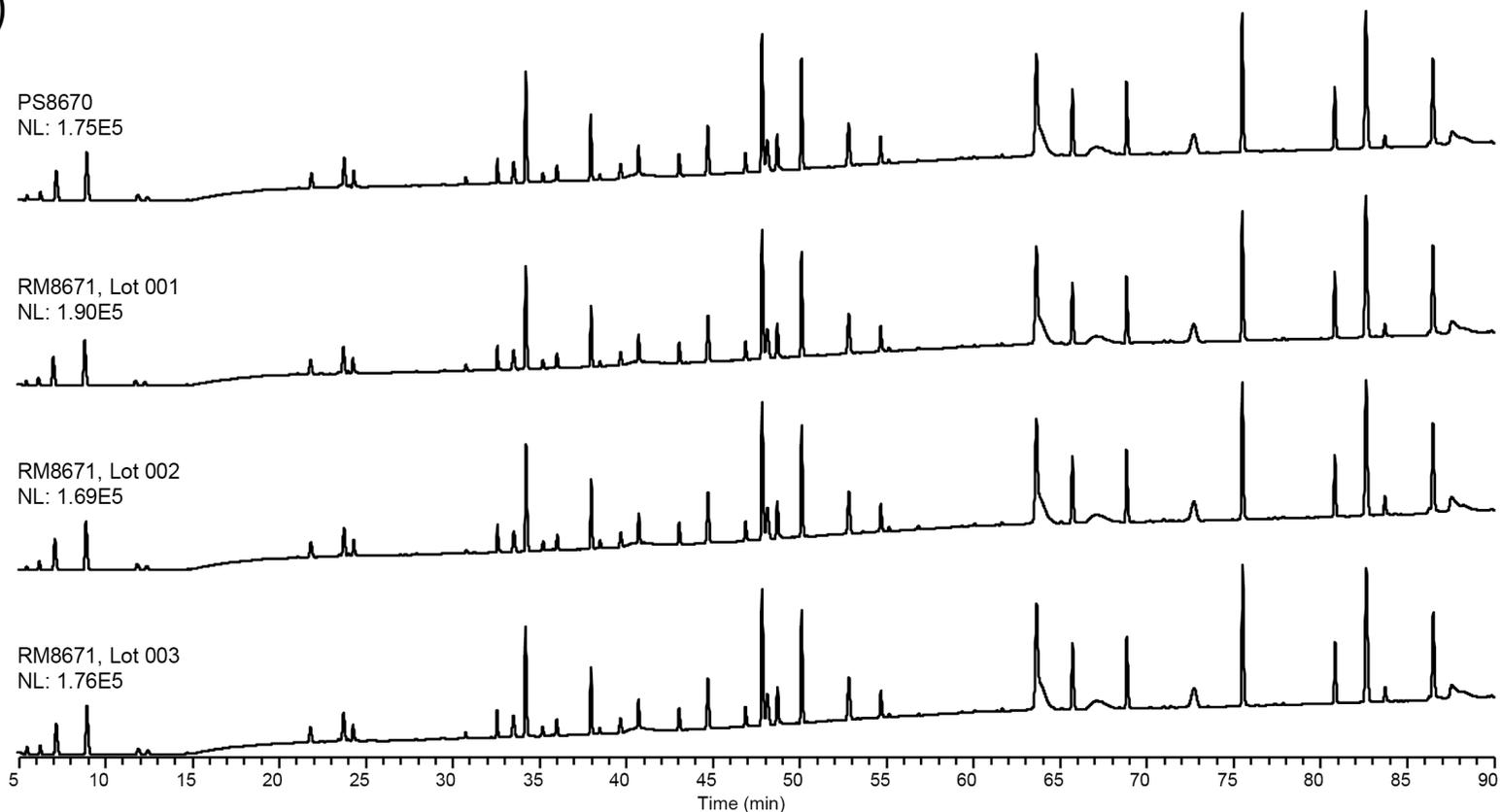
Figure 21 (continued) Alignment of PS 8670 with chromatograms lots 14HB-D-001, 14HB-D-002, and 14HB-D-003. Tryptic digests of the three RM lots were analyzed by LC-UV-MS and the similarity of the resulting A) TIC and B) UV chromatograms compared against the reference peptide map generated from the PS 8670 digest as depicted in Figure 21 (top trace of each panel). The initial five minutes of the UV traces are not shown due to the large difference in scale between the relative levels of absorbance during peaks detected during the 0 min to 5 min period and the 5 min to 90 min period

6. Conclusions

Samples were analyzed throughout this report using a variety of analytical methods to evaluate physiochemical properties for three lots of RM 8671. Each assay showed that all vials of lots 14HB-D-001, 14HB-D-002, and 14HB-D-003 were homogeneous with respect to concentration and physiochemical properties. Some methods (capillary electrophoresis and dynamic light scattering) required minor alterations in uncertainty budget to account for long-term intermediate precision as detailed above. RM 8671 is homogeneous and stable and will continue to undergo regular stability monitoring as part of the lifecycle management plan.

References

[1]   Schiel JE , Turner A (2018) The NISTmAb Reference Material 8671 lifecycle management and quality plan. *Anal Bioanal Chem* 410(8):2067-2078. https://doi.org/10.1007/s00216-017-0844-2

[2]   Turner A , Schiel JE (2018) Qualification of NISTmAb charge heterogeneity control assays. *Anal Bioanal Chem* 410(8):2079-2093. https://doi.org/10.1007/s00216-017-0816-6

[3]   Turner A, Yandrofski K, Telikepalli S, King J, Heckert A, Filliben J, Ripple D, Schiel JE (2018) Development of orthogonal NISTmAb size heterogeneity control methods. *Anal Bioanal Chem* 410(8):2095-2110. https://doi.org/10.1007/s00216-017-0819-3

[4]   Formolo T, Mellisa L, Michaella L, Lisa K, Scott L, Karen P, Lisa M, Kurt B, Michael B, Darryl D, John S (2015) Determination of the NISTmAb Primary Structure. *State-of-the-Art and Emerging Technologies for Therapeutic Monoclonal Antibody Characterization Volume 2 Biopharmaceutical Characterization: The NISTmAb Case Study,* ACS Symposium Series (American Chemical Society), Vol. 1201, Chapter 1 pp 1-62.

[5]   Schiel JE, Turner A, Mouchahoir T, Yandrofski K, Telikepalli S, King J, DeRose P, Ripple D, Phinney K (2018) The NISTmAb Reference Material 8671 value assignment, homogeneity, and stability. *Anal Bioanal Chem* 410(8):2127-2139. https://doi.org/10.1007/s00216-017-0800-1

[6]   Beauchamp CR, Camara JE, Carney J, Choquette SJ, Cole KD, DeRose PC, Duewer DL, Epstein MS, Kline MC, Lippa KA (2020) Metrological Tools for the Reference Materials and Reference Instruments of the NIST Material Measurement Laboratory. *NIST Special Publication* 260:136.

[7]   Formolo T, Ly M, Levy M, Kilpatrick L, Lute S, Phinney K, Marzilli L, Brorson K, Boyne M, Davis D, Schiel J (2015) Determination of the NISTmAb Primary Structure. *State-of-the-Art and Emerging Technologies for Therapeutic Monoclonal Antibody Characterization Volume 2 Biopharmaceutical Characterization: The NISTmAb Case Study,* ACS Symposium Series (American Chemical Society), Vol. 1201, Chapter 1 pp 1-62.

[8]   Gokarn Y, Agarwal S, Arthur K, Bepperling A, Day ES, Filoti D, Greene DG, Hayes D, Kroe-Barrett R, Laue T, Lin J, McGarry B, Razinkov V, Singh S, Taing R, Venkataramani S, Weiss W, Yang D, Zarraga IE (2015) Biophysical Techniques for Characterizing the Higher Order Structure and Interactions of Monoclonal Antibodies. *State-of-the-Art and Emerging Technologies for Therapeutic Monoclonal Antibody Characterization Volume 2 Biopharmaceutical Characterization: The NISTmAb Case Study,* ACS Symposium Series (American Chemical Society), Vol. 1201, Chapter 6 pp 285-327.

[9]   Schiel JE, Davis DL, Borisov OB eds (2015) *State-of-the-Art and Emerging Technologies for Therapeutic Monoclonal Antibody Characterization Volume 2. Biopharmaceutical Characterization: The NISTmAb Case Study* (American Chemical Society), Vol. 1201, p 427.

[10]   Ripple DC , DeRose PC (2018) Primary determination of particle number concentration with light obscuration and dynamic imaging particle counters. *Journal of Research of the National Institute of Standards and Technology* 123:1-21.

[11]   Pace CN, Vajdos F, Fee L, Grimsley G, Gray T (1995) How to measure and predict the molar absorption coefficient of a protein. *Protein Sci* 4(11):2411-2423. https://doi.org/10.1002/pro.5560041120

[12]   Mouchahoir T , Schiel JE (2018) Development of an LC-MS/MS peptide mapping protocol for the NISTmAb. *Anal Bioanal Chem* 410(8):2111-2126. https://doi.org/10.1007/s00216-018-0848-6

[13]   Parminder K, Janna K, Wuxian S, Sichun Y, Mark RC (2015) Covalent Labeling Techniques for Characterizing Higher Order Structure of Monoclonal Antibodies. *State-of-the-Art and Emerging Technologies for Therapeutic Monoclonal Antibody Characterization Volume 3 Defining the Next Generation of Analytical and Biophysical Techniques,* ACS Symposium Series (American Chemical Society), Vol. 1202, Chapter 3 pp 45-73.

Appendix A: Supplemental Materials

Table A1. 5YSVmass concentration values determined for RM 8671 lots using UV-Vis spectrophotometry (*n* = 10).

Lot	14HB-D-001	14HB-D-002	14HB-D-003
Concentration	10.04317638	10.0039	10.02306
	10.04732168	10.06961	10.00524
	10.04556173	10.00892	10.03685
	10.08600109	10.01601	9.982878
	10.06842052	10.01182	10.01294
	10.04335746	10.02894	10.01268
	10.04204182	10.02195	10.04001
	10.03767367	10.05922	10.06652
	10.08549248	10.02029	10.01168
	10.04667128	10.02308	10.01196
Average	**10.055**	**10.026**	**10.020**

Table A2. 5YSV SEC Results for RM 8671 Lots (*n* = 3 vials)[a]

	8670	14HB-D-001	14HB-D-002	14HB-D-003
Monomeric Purity (%)	98.748	96.658	96.512	96.690
	98.744	96.652	96.505	96.721
	98.740	96.633	96.501	96.703
	98.744	**96.647**	**96.505**	**96.705**
High Molecular Weight RA (%)	1.045	3.142	3.209	3.112
	1.052	3.170	3.296	3.079
	1.052	3.152	3.301	3.099
	1.050	**3.155**	**3.296**	**3.097**
Low Molecular Weight RA (%)	0.208	0.201	0.198	0.198
	0.204	0.196	0.199	0.200
	0.207	0.197	0.198	0.198
	0.206	**0.198**	**0.198**	**0.199**

[a]*Values for each individual injection along with the average of 3 injections for each lot (rack 1, 50, and 90) in bold.*

Table A3. 5YSV CE-SDS results for RM 8671 Lots (*n* = 3 vials)[a]

	8670	14HB-D-001	14HB-D-002	14HB-D-003
Monomeric Purity (%)	99.690	99.610	99.612	99.690
	99.071	99.504	98.544	99.071
	99.354	99.199	98.747	99.354
	99.372	**99.438**	**98.967**	**99.372**
Thioether RA (%)	0.365	0.296	0.359	0.322
	0.349	0.361	0.329	0.359
	0.328	0.341	0.314	0.333
	0.347	**0.333**	**0.334**	**0.338**
Glycan Occupancy (%)	99.320	99.354	99.280	99.306
	99.284	99.300	99.426	99.206
	99.298	99.310	99.369	99.367
	99.300	**99.321**	**99.359**	**99.293**

[a]*Values for each individual injection along with the average of 3 injections for each lot (rack 1, 50, and 90) in bold.*

Table A4. 5YSV CZE Results for PS 8670 and RM 8671 (*n* = 3 vials)[a]

	8670	14HB-D-001	14HB-D-002	14HB-D-003
Charge Purity (%)	74.403	73.380	72.864	73.282
	74.223	72.998	72.340	73.224
	74.443	73.645	72.885	73.697
	74.356	**73.341**	**72.696**	**73.401**
Acidic Variants RA (%)	16.739	16.393	16.547	16.419
	16.791	16.727	17.386	16.638
	16.857	16.365	16.635	16.214
	16.796	**16.495**	**16.856**	**16.423**
Basic Variants RA (%)	8.858	10.228	10.589	10.299
	8.985	10.275	10.274	10.138
	8.700	9.990	10.481	10.089
	8.848	**10.164**	**10.448**	**10.176**

[a]*Values for each individual injection along with the average of 3 injections for each lot (rack 1, 50, and 90) in bold.*

Table A5: 2020 DLS results for RM 8671 lots (n=9, 3 vials and 3 runs from each vial)[a]

	200 nm beads	8670	14 HB-D-001	14 HB-D-002	14 HB-D-003
Hydrodynamic Diameter (nm) Rack 1	201.4	10.09	9.85	9.58	9.36
	205	10.12	9.96	9.31	9.44
	203.6	10.11	9.92	9.29	9.51
	203.33	**10.11**	**9.91**	**9.39**	**9.44**
Hydrodynamic Diameter (nm) Rack 50	200.3	9.58	9.41	9.48	9.15
	203.4	9.67	9.37	9.37	9.24
	203.1	9.68	9.28	9.42	9.28
	202.27	**9.65**	**9.35**	**9.42**	**9.22**
Hydrodynamic Diameter (nm) Rack 90	203.9	9.59	9.14	9.11	9.35
	205.3	9.69	9.31	9.40	9.33
	203.2	9.76	9.39	9.42	9.47
	204.13	**9.68**	**9.28**	**9.31**	**9.39**
Global Average	**203.2**	**9.81**	**9.51**	**9.38**	**9.35**

[a]*Values for each individual injection along with the average of 3 injections for each lot (rack 1, 50, and 90) in bold.*

Table A6: 2020 FI results for RM 8671 lots. (PS 8670, n=5, 5 vials and 1 run from each vial; RM 8671 n=6, 6 vials and 1 run from each vial)[a]

Samples	5 μm Count-Cal beads	PS 8670	14 HB-D-001	14 HB-D-002	14 HB-D-003
N (≥2 μm), mL^{-1}	3266.57	3528.00	9227.67	5971.45	6491.72
	3188.92	4252.75	9781.59	4554.17	5945.57
	3323.52	3991.32	7032.70	5810.97	6740.21
	3383.05	6015.45	5369.27	7296.72	10213.85
	3300.22	3197.72	6546.08	7014.58	7858.40
	3364.93		6719.50	5278.19	7335.54
Average	**3304.54**	**4197.05**	**7446.13**	**5987.68**	**7430.88**

[a]*Values listed in bold represent the average of the measurements for each sample (from rack 1, 50, and 90).*

A)

B)
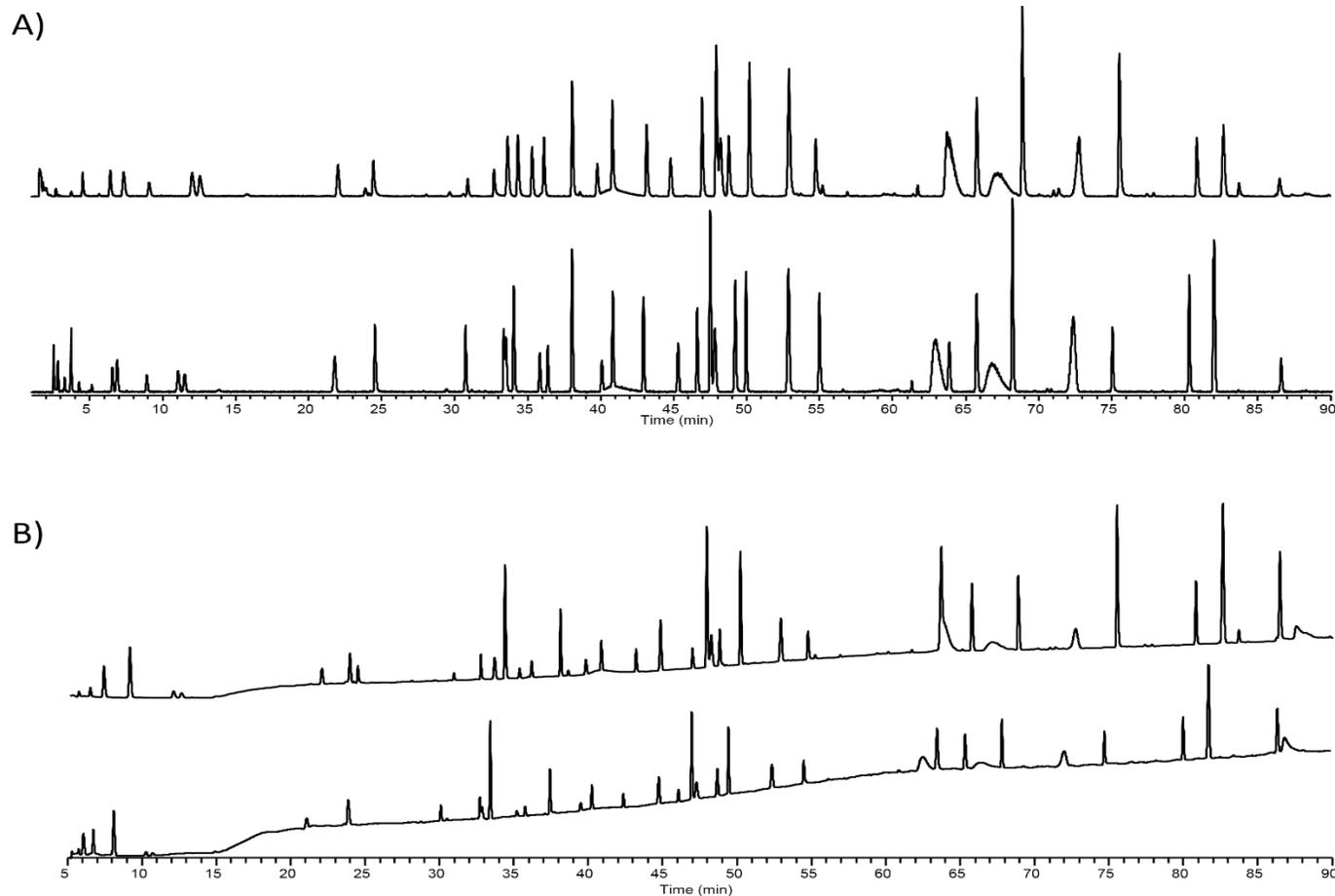
Figure A1. Comparison of PS 8670 reference peptide maps. PS 8670 Peptide maps generated by LC-UV-MS analysis for the original certification and the current recertification were compared. Panel A shows TIC peaks from MS analysis and Panel B shows peaks from UV (214 nm) analysis. Zoomed views of the TIC spectra (Panels C through G) and UV spectra (Panels F through L) are shown with peak retention times labeled as they correspond to Table A7. The initial five minutes of the UV traces are not shown in Panel B and due to the large difference in scale between the relative levels of absorbance of peaks detected during the 0 min to 5 min period and the 5 min to 90 min period. This time period is depicted in Panel C. The top trace in each panel represents the current data set and the bottom trace represents the original data set.

C)

Figure A1 (continued). Comparison of PS 8670 reference peptide maps. PS 8670 Peptide maps generated by LC-UV-MS analysis for the original certification and the current recertification were compared. Panel A shows TIC peaks from MS analysis and Panel B shows peaks from UV (214 nm) analysis. Zoomed views of the TIC spectra (Panels C through G) and UV spectra (Panels F through L) are shown with peak retention times labeled as they correspond to Table A7. The initial five minutes of the UV traces are not shown in Panel B and due to the large difference in scale between the relative levels of absorbance of peaks detected during the 0 min to 5 min period and the 5 min to 90 min period. This time period is depicted in Panel C. The top trace in each panel represents the current data set and the bottom trace represents the original data set.

D)

Figure A1 (continued). Comparison of PS 8670 reference peptide maps. PS 8670 Peptide maps generated by LC-UV-MS analysis for the original certification and the current recertification were compared. Panel A shows TIC peaks from MS analysis and Panel B shows peaks from UV (214 nm) analysis. Zoomed views of the TIC spectra (Panels C through G) and UV spectra (Panels F through L) are shown with peak retention times labeled as they correspond to Table A7. The initial five minutes of the UV traces are not shown in Panel B and due to the large difference in scale between the relative levels of absorbance of peaks detected during the 0 min to 5 min period and the 5 min to 90 min period. This time period is depicted in Panel C. The top trace in each panel represents the current data set and the bottom trace represents the original data set.

E)

Figure A1 (continued). Comparison of PS 8670 reference peptide maps. PS 8670 Peptide maps generated by LC-UV-MS analysis for the original certification and the current recertification were compared. Panel A shows TIC peaks from MS analysis and Panel B shows peaks from UV (214 nm) analysis. Zoomed views of the TIC spectra (Panels C through G) and UV spectra (Panels F through L) are shown with peak retention times labeled as they correspond to Table A7. The initial five minutes of the UV traces are not shown in Panel B and due to the large difference in scale between the relative levels of absorbance of peaks detected during the 0 min to 5 min period and the 5 min to 90 min period. This time period is depicted in Panel C. The top trace in each panel represents the current data set and the bottom trace represents the original data set.

F)

**Figure A1** (continued). Comparison of PS 8670 reference peptide maps. PS 8670 Peptide maps generated by LC-UV-MS analysis for the original certification and the current recertification were compared. Panel A shows TIC peaks from MS analysis and Panel B shows peaks from UV (214 nm) analysis. Zoomed views of the TIC spectra (Panels C through G) and UV spectra (Panels F through L) are shown with peak retention times labeled as they correspond to Table A7. The initial five minutes of the UV traces are not shown in Panel B and due to the large difference in scale between the relative levels of absorbance of peaks detected during the 0 min to 5 min period and the 5 min to 90 min period. This time period is depicted in Panel C. The top trace in each panel represents the current data set and the bottom trace represents the original data set

G)

Figure A1 (continued). Comparison of PS 8670 reference peptide maps. PS 8670 Peptide maps generated by LC-UV-MS analysis for the original certification and the current recertification were compared. Panel A shows TIC peaks from MS analysis and Panel B shows peaks from UV (214 nm) analysis. Zoomed views of the TIC spectra (Panels C through G) and UV spectra (Panels F through L) are shown with peak retention times labeled as they correspond to Table A7. The initial five minutes of the UV traces are not shown in Panel B and due to the large difference in scale between the relative levels of absorbance of peaks detected during the 0 min to 5 min period and the 5 min to 90 min period. This time period is depicted in Panel C. The top trace in each panel represents the current data set and the bottom trace represents the original data set.

H)

Figure A1 (continued). Comparison of PS 8670 reference peptide maps. PS 8670 Peptide maps generated by LC-UV-MS analysis for the original certification and the current recertification were compared. Panel A shows TIC peaks from MS analysis and Panel B shows peaks from UV (214 nm) analysis. Zoomed views of the TIC spectra (Panels C through G) and UV spectra (Panels F through L) are shown with peak retention times labeled as they correspond to Table A7. The initial five minutes of the UV traces are not shown in Panel B and due to the large difference in scale between the relative levels of absorbance of peaks detected during the 0 min to 5 min period and the 5 min to 90 min period. This time period is depicted in Panel C. The top trace in each panel represents the current data set and the bottom trace represents the original data set.

l)

Figure A1 (continued). Comparison of PS 8670 reference peptide maps. PS 8670 Peptide maps generated by LC-UV-MS analysis for the original certification and the current recertification were compared. Panel A shows TIC peaks from MS analysis and Panel B shows peaks from UV (214 nm) analysis. Zoomed views of the TIC spectra (Panels C through G) and UV spectra (Panels F through L) are shown with peak retention times labeled as they correspond to Table A7. The initial five minutes of the UV traces are not shown in Panel B and due to the large difference in scale between the relative levels of absorbance of peaks detected during the 0 min to 5 min period and the 5 min to 90 min period. This time period is depicted in Panel C. The top trace in each panel represents the current data set and the bottom trace represents the original data set.

J)

UV: 214 nm
NL: 1.54E5
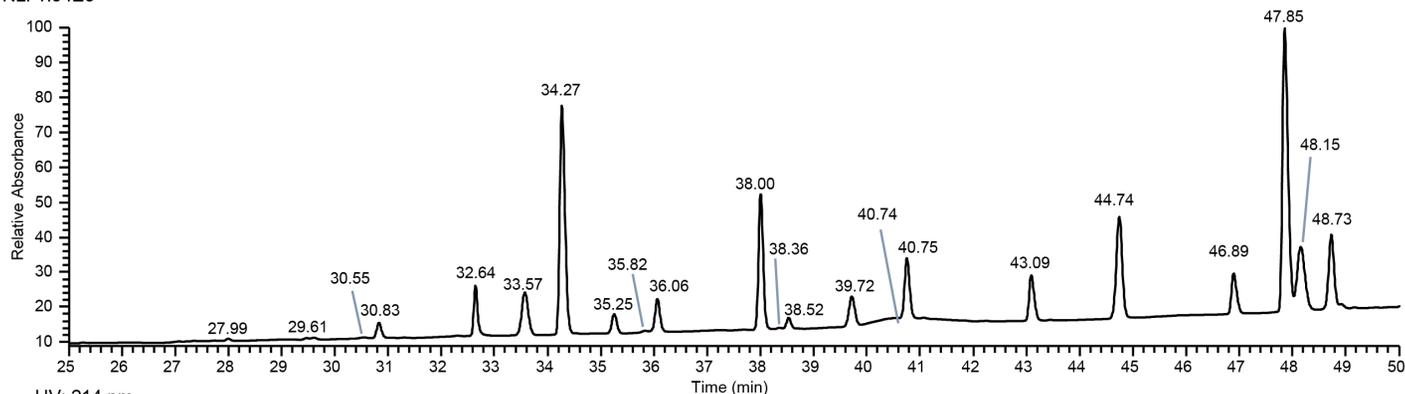

UV: 214 nm
NL: 6.89E4

Figure A1 (continued). Comparison of PS 8670 reference peptide maps. PS 8670 Peptide maps generated by LC-UV-MS analysis for the original certification and the current recertification were compared. Panel A shows TIC peaks from MS analysis and Panel B shows peaks from UV (214 nm) analysis. Zoomed views of the TIC spectra (Panels C through G) and UV spectra (Panels F through L) are shown with peak retention times labeled as they correspond to Table A7. The initial five minutes of the UV traces are not shown in Panel B and due to the large difference in scale between the relative levels of absorbance of peaks detected during the 0 min to 5 min period and the 5 min to 90 min period. This time period is depicted in Panel C. The top trace in each panel represents the current data set and the bottom trace represents the original data set.

K)

Figure A1 (continued). Comparison of PS 8670 reference peptide maps. PS 8670 Peptide maps generated by LC-UV-MS analysis for the original certification and the current recertification were compared. Panel A shows TIC peaks from MS analysis and Panel B shows peaks from UV (214 nm) analysis. Zoomed views of the TIC spectra (Panels C through G) and UV spectra (Panels F through L) are shown with peak retention times labeled as they correspond to Table A7. The initial five minutes of the UV traces are not shown in Panel B and due to the large difference in scale between the relative levels of absorbance of peaks detected during the 0 min to 5 min period and the 5 min to 90 min period. This time period is depicted in Panel C. The top trace in each panel represents the current data set and the bottom trace represents the original data set.

L)

Figure A1 (continued). Comparison of PS 8670 reference peptide maps. PS 8670 Peptide maps generated by LC-UV-MS analysis for the original certification and the current recertification were compared. Panel A shows TIC peaks from MS analysis and Panel B shows peaks from UV (214 nm) analysis. Zoomed views of the TIC spectra (Panels C through G) and UV spectra (Panels F through L) are shown with peak retention times labeled as they correspond to Table A7. The initial five minutes of the UV traces are not shown in Panel B and due to the large difference in scale between the relative levels of absorbance of peaks detected during the 0 min to 5 min period and the 5 min to 90 min period. This time period is depicted in Panel C. The top trace in each panel represents the current data set and the bottom trace represents the original data set.

Heavy Chain (96 %)

```
        10   20   30   40   50   60   70   80   90
QVTLRESGPA LVKPTQTLTL TCTFSGFSLS TAGMSVGWIR QPPGKALEWL ADIWWDDKKH YNPSLKDRLT ISKDTSKNQV VLKVTNMDPA

       100   110   120   130   140   150   160   170   180
DTATYYCARD MIFNFYFDVW GQGTTVTVSS ASTKGPSVFP LAPSSKSTSG GTAALGCLVK DYFPEPVTVS WNSGALTSGV HTFPAVLQSS

       190   200   210   220   230   240   250   260   270
GLYSLSSVVT VPSSSLGTQT YICNVNHKPS NTKVDKRVEP KSCDKTHTCP PCPAPELLGG PSVFLFPPKP KDTLMISRTP EVTCVVVDVS

       280   290   300   310   320   330   340   350   360
HEDPEVKFNW YVDGVEVHNA KTKPREEQYN STYRVVSVLT VLHQDWLNGK EYKCKVSNKA LPAPIEKTIS KAKGQPREPQ VYTLPPSREE

       370   380   390   400   410   420   430   440   450
MTKNQVSLTC LVKGFYPSDI AVEWESNGQP ENNYKTTPPV LDSDGSFFLY SKLTVDKSRW QQGNVFSCSV MHEALHNHYT QKSLSLSPGK
```

**Light Chain (99 %)**

```
        10         20         30         40         50         60         70         80         90
DIQMTQSPST LSASVGDRVT ITCSASSRVG YMHWYQQKPG KAPKLLIYDT SKLASGVPSR FSGSGSGTEF TLTISSLQPD DFATYYCFQG

       100        110        120        130        140        150        160        170        180
SGYPFTFGGG TKVEIKRTVA APSVFIFPPS DEQLKSGTAS VVCLLNNFYP REAKVQWKVD NALQSGNSQE SVTEQDSKDS TYSLSSTLTL

       190        200        210
SKADYEKHKV YACEVTHQGL SSPVTKSFNR GEC
```

Figure A2. PS 8670 sequence coverage. PS 8670 tryptic digest was analyzed by UHPLC-UV-MS/MS and sequence coverage of the heavy and light chains was calculated after peptide identification. The amino acid sequence is shown with underlining to indicate the confirmed regions.

Table A7. Identification of ions contributing to TIC and UV chromatogram peaks. A peptide map of PS8670 was generated from tryptic digestion of PS 8670 followed by LC-UV-MS analysis. A second injection of the digest was analyzed by LC-UV-MS/MS for confident identification of the peptides. These identifications were mapped to the TIC and UV peaks in Figure 21 (top trace of each panel) and are compared to the identifications mapped to the TIC and UV peaks in the original peptide map in Figure 21 (bottom trace of each panel). Relative Intensity within Peak = the relative contribution of each ion within the peak to the total TIC peak signal; contributions are categorized as Predominant (approximately > 70 % of the total peak signal), Major (approximately 70 % to 40 % of the total peak signal), Substantial (approximately 40 % to 20 % of the total peak signal), Minor (approximately 20 % to 5 % of the total peak signal), or Trace (5 % or less of the total peak signal). All cysteine residues are carbamidomethylated unless noted as having a missed alkylation.

Current MS Peak Apex Time [13]	Current UV Peak Apex Time [13]	Original MS Peak Apex Time [13]	Original UV Peak Apex Time [13]	Sequence	Mod. Summary	Relative Intensity within Peak	Comment
1.58	n.d.	1.55	n.d.	Buffer Component (327 m/z cluster)		Predominant	
				Unknown (457 m/z)		Substantial	Also present in original map, thought to also be a buffer component
1.80	1.76	1.87	1.78	TISK		Substantial	Predominant ions are buffer components
				APK		Minor	
				QPPGK		Minor	
				VEPK		Minor	
				GQPR		Minor	
				VDKR		Minor	
				EAK		Minor	
				EYK		Trace	
				RVEPK		Trace	
				TKPR		Minor	
n.d.	1.86	n.d.	1.89	Buffer components			
2.69	2.63	2.32	n.d.	EEMTK		Major	
		2.73	n.d.	ADYEK		Predominant	

Current MS Peak Apex Time [13]	Current UV Peak Apex Time [13]	Original MS Peak Apex Time [13]	Original UV Peak Apex Time [13]	Sequence	Mod. Summary	Relative Intensity within Peak	Comment
		2.79	2.71	SFNR		Predominant	Previously resolved, now co-eluting
				NKPGVYTK (Trypsin)		Trace	
3.74	3.67			Unknown (390 m/z)		Predominant	Present in original data, but below TIC threshold
4.52	4.46	4.19	n.d.	VEIK		Predominant	
5.66	5.59			Unknown (445 m/z)		Predominant	New peak (445 and 333 present in original data < 1% of the total peak comprising HYNPSLK, WYQQKPGK)
				Unknown (333 m/z)		Predominant	
				Unknown (324 m/z)		Major	
6.42	6.35	5.61	5.55	LTVDK		Predominant	
7.32	7.27	5.94	5.86	HYNPSLK		Predominant	
				WYQQKPGK		Trace	
9.08	9.02	7.98	7.91	VQWK		Predominant	
				QVTLR		Trace	New peak component
12.03	11.95	10.14	10.07	NQVVLK		Predominant	

Current MS Peak Apex Time [13]	Current UV Peak Apex Time [13]	Original MS Peak Apex Time [13]	Original UV Peak Apex Time [13]	Sequence	Mod. Summary	Relative Intensity within Peak	Comment
12.55	12.49	10.58	10.51	LTISK		Predominant	
n.d.	14.83	n.d.	14.74	Unknown			
15.78	15.74	12.92	n.d.	DRLTISK		Predominant	
n.d.	21.2			Unknown			
22.01	21.95	21.01	20.94	LASGVPSR		Predominant	
n.d.	21.2			Unknown			
23.90	23.82	23.81	23.75	EEQYnSTYR	A2G0F	Predominant	Previously co-eluted with VTITCSASSR, now resolved
				EEQYnSTYR	A2G1F	Predominant	
				EEQYnSTYR	A2G2F	Minor	
				APVLSDSSCK (Trypsin)		Minor	New peak component
24.14	24.08			SVMHEALHNHYTQK		Predominant	New peak
24.44	24.37	23.81	23.75	VTITCSASSR		Predominant	Previously co-eluted with EEQYnSTYR glycopeptides, now resolved
28.07	27.99	27.17	27.12	SCSVMHEALHNHYTQK		Predominant	
29.68	29.61	28.75	28.67	SLSLSPGK		Predominant	Previously resolved, now co-eluting
				VGYmHWYQQKPGK	Oxidation (M34)	Minor	
30.58	30.55	30.07	30	LSSPATLNSR (Trypsin)		Predominant	Previously co-eluted with HKVYACEVTHQGLSSPVTK, now resolved

Current MS Peak Apex Time [13]	Current UV Peak Apex Time [13]	Original MS Peak Apex Time [13]	Original UV Peak Apex Time [13]	Sequence	Mod. Summary	Relative Intensity within Peak	Comment
				APVLSDSScK (Trypsin)	DTT (C156)	Minor	New peak component (present at low level in original data, but below TIC threshold)
30.91	30.83	30.07	30	HKVYACEVTHQGLSSPVTK		Predominant	
				EPQVY		Trace	New peak component (present at low level in original data, but below TIC threshold)
32.71	32.64	32.71	32.64	VDNALQSGNSQESVTEQDSK		Predominant	
33.62	33.57	32.84	32.78	ALPAPIEK		Predominant	
34.34	34.27	33.4	33.33	VGYMHWYQQKPGK		Predominant	
35.32	35.25	35.2	35.13	qVTLR	Gln -> pyroGlu (Q1)	Predominant	Previously co-eluted with VATVSLPR, now resolved
35.95	35.82			VATVSLPR (Trypsin)		Predominant	Previously co-eluted with qVTLR (Gln -> pyroGlu), now resolved
				SVGWIR		Minor	New peak component (present at low level in original

Current MS Peak Apex Time [13]	Current UV Peak Apex Time [13]	Original MS Peak Apex Time [13]	Original UV Peak Apex Time [13]	Sequence	Mod. Summary	Relative Intensity within Peak	Comment
							data, but below TIC threshold)
36.12	36.06	35.77	35.69	DTLMISR		Predominant	
38.08	38	37.45	37.37	VYACEVTHQGLSSPVTK		Predominant	Previously co-eluted with VGYMHWYQQK, now resolved
				LASGVPsR	Dehydration (S59)	Trace	New peak component
38.43	38.36			VFSCSVMHEALHNHYTQK		Predominant	New peak component (present in original data at < 1 % of TIC peak)
38.59	38.52	37.45	37.37	VGYMHWYQQK		Predominant	Previously co-eluted with VYACEVTHQGLSSPVTK, now resolved
39.76	39.72	39.52	39.43	SLSLSPGk	Lys-loss (K450)	Predominant	
				TVLHQDWLNGK		Trace	
40.81	40.74	40.26	n.d.	EPQVYTLPPSR		Predominant	
		40.26	n.d.	WQQGNVFSCSVmHEALHNHYTQK	Oxidation (M431)	Trace	
		42.38	42.31	DIQmTQSPSTLSASVGDR	Oxidation (M4)	Trace	Previously co-eluted with

Current MS Peak Apex Time [13]	Current UV Peak Apex Time [13]	Original MS Peak Apex Time [13]	Original UV Peak Apex Time [13]	Sequence	Mod. Summary	Relative Intensity within Peak	Comment
							STSGGTAALGCLVK
				GTAALGCLVK		Trace	New peak component
				VYAcEVTHQGLSSPVTK	Missed Alkylation (C193)	Trace	New peak component
				SLSSTLTLSK		Trace	New peak component
				IFPPSDEQLK		Trace	New peak component
40.82	40.75	40.26	40.18	LLIYDTSK		Predominant	
43.14	43.09	42.38	42.31	STSGGTAALGCLVK		Predominant	Previously co-eluted with DIQmTQSPSTLSASVGDR+Ox
44.79	44.74	44.77	44.7	VTNMDPADTATYYCAR		Predominant	
46.95	46.89	46.1	46.02	NQVSLTCLVK		Predominant	
47.91	47.85	46.98	46.92	WQQGNVFSCSVMHEALHNHYTQK		Predominant	
48.21	48.15	47.3	47.24	GPSVFPLAPSSK		Predominant	
48.77	48.73	48.72	48.66	DIQMTQSPSTLSASVGDR		Predominant	
				WQQGNVFSC		Trace	
				STAGMSVGWIR		Trace	Present in original data, but resolved and below TIC threshold
50.18	50.12	49.47	49.4	FNWYVDGVEVHNAK		Predominant	

Current MS Peak Apex Time [13]	Current UV Peak Apex Time [13]	Original MS Peak Apex Time [13]	Original UV Peak Apex Time [13]	Sequence	Mod. Summary	Relative Intensity within Peak	Comment
52.90	52.83	52.4	52.33	TPEVTCVVVDVSHEDPEVK		Predominant	
53.41	53.31			FNWYVDGVEVHnAK	Ammonia-loss (N289)	Substantial	Present in original data, but below TIC threshold
				Unknown (719 m/z)		Predominant	Present in original data at trace level, but believed to have been in-source event generated from TPEVTCVVVDVSHEDPEVK
53.71	53.67			TPEVTcVVVDVSHEDPEVK	Missed Alkylation (C264)	Predominant	New peak
54.72	54.67	54.55	54.48	DSTYSLSSTLTLSK		Predominant	Previously co-eluted with LGEHNIDVLEGNEQFINAAK and nQVSLTCLVK (deamidated), now resolved
55.20	55.15			LGEHNIDVLEGNEQFINAAK (Trypsin)		Predominant	Previously co-eluted with DSTYSLSSTLTLSK, now resolved
				nQVSLTCLVK	Deamidation (N364)	Trace	Previously co-eluted with DSTYSLSSTLTLSK, now resolved

Current MS Peak Apex Time [13]	Current UV Peak Apex Time [13]	Original MS Peak Apex Time [13]	Original UV Peak Apex Time [13]	Sequence	Mod. Summary	Relative Intensity within Peak	Comment
				TLDNDIMLIK (Trypsin)		Trace	New peak component
				Unknown (883 m/z)		Substantial	New peak component (present in original data at ≈ 2.5 % of TIC peak)
56.90	56.84	56.18	56.12	SLSTAGMSVGWIR		Predominant	
59.38	59.33	58.66	n.d.	Unknown (830 m/z)		Predominant	Misidentified as GPSVFPLAPSSK STSGGTAALGC LVK in original data due to incorrect charge state assignment; previously co-eluted with RTVAAPSVFIFP PSDEQLK, IITHPNFNGNTL DNDImLIK+Ox
59.56	59.52			RTVAAPSVFIFPPSDEQLK		Predominant	
60.12	60.07	59.96	n.d.	FNWYVDGVEVH		Predominant	
61.41	61.36			Unknown (1054 m/z)		Predominant	New peak (present in original data, but below TIC threshold)
				fNWYVDGVEVHNAK	Carbamylation (F278)	Substantial	New peak

Current MS Peak Apex Time [13]	Current UV Peak Apex Time [13]	Original MS Peak Apex Time [13]	Original UV Peak Apex Time [13]	Sequence	Mod. Summary	Relative Intensity within Peak	Comment
				TPEVTCVVVDVSHEDPEVK	Dehydration	Substantial	New peak (present in original data, but below TIC threshold)
61.73	61.66	60.96	60.87	IITHPNFNGNTLDNDIMLIK (Trypsin)		Predominant	
63.73	63.63	62.58	62.48	ESGPALVKPTQTLTLTCTF		Trace	Previously resolved from GFYPSDIAVEW ESNGQPENNYK
		63.54	63.46	GFYPSDIAVEWESNGQPENNY K		Substantial	Previously resolved from ESGPALVKPTQ TLTLTCTF and THTCPPCPAPEL LGGPSVFLFPPK PK
63.90	63.81	62.58	62.48	THTCPPCPAPELLGGPSVFLFPP KPK		Predominant	Previously resolved from GFYPSDIAVEW ESNGQPENNYK
				SGTASVVCLLnNFYPR	Deamidation (N136)	Trace	New peak component
65.77	65.7	65.42	65.35	TTPPVLDSDGSFFLYSK		Predominant	
67.21	67.07	66.52	66.43	TVAAPSVFIFPPSDEQLK		Predominant	
				Unknown (1137 m/z)		Trace	New peak component
				LLIYDTSK	Dehydration	Trace	New peak component

Current MS Peak Apex Time [13]	Current UV Peak Apex Time [13]	Original MS Peak Apex Time [13]	Original UV Peak Apex Time [13]	Sequence	Mod. Summary	Relative Intensity within Peak	Comment
68.88	68.82	67.91	67.84	VVSVLTVLHQDWLNGK		Predominant	Previously co-eluted with SGFSLSTAGMSVGWIR, now resolved
71.03	70.97	70.61	70.52	ESGPALVKPTQTLTLTCTFSGF		Predominant	Previously eluted after VVSVLTVLHQDWLnGK (ammonia-loss)
				DYFPEPVTVSWNSGALTSGVH		Minor	New peak component (present in original data, but resolved and below TIC threshold)
71.40	71.33	70.32	70.25	VVSVLTVLHQDWLnGK	Ammonia-loss (N318)	Predominant	Previously eluted before ESGPALVKPTQTLTLTCTFSGF
72.76	72.68	72.1	72.03	SGTASVVCLLNNFYPR		Predominant	
75.54	75.47	74.82	74.74	ALEWLADIWWDDKK		Predominant	
				ESGPALVKPTQTLTLTCTFSGFSLSTAGMSVGWIRQPPGK		Trace	
77.43	77.36			ESGPALVKPTQTLTLTCTFSGFSLSTAGmSVGWIR	Oxidation (M34)	Predominant	New peak (present in original data, but below TIC threshold)
77.87	77.83			VcNYVNWIQQTIAAN (Trypsin)	DTT (C218)	Predominant	New peak (present in original data,

Current MS Peak Apex Time [13]	Current UV Peak Apex Time [13]	Original MS Peak Apex Time [13]	Original UV Peak Apex Time [13]	Sequence	Mod. Summary	Relative Intensity within Peak	Comment
							but below TIC threshold)
				ESGPALVKPTQTLTLTCTFSGF SLSTAGM		Predominant	New peak (present in original data, but below TIC threshold)
80.85	80.78	80.14	80.06	ESGPALVKPTQTLTLTCTFSGF SLSTAGMSVGWIR		Predominant	
82.66	82.59	81.87	81.78	DYFPEPVTVSWNSGALTSGVH TFPAVLQSSGLYSLSSVVTVPS SSLGTQTYICNVNHKPSNTK		Predominant	
83.74	83.67	83.54	83.45	ALEWLADIWWDDK		Predominant	
86.31	86.22			DYFPEPVTVSWNSGALTSGVH TFPAVLQSSGLYSLSSVVTVPS SSLGTQTYICNVNHK		Predominant	New peak (present in original data, but below TIC threshold)
86.51	86.44	86.51	86.42	FSGSGSGTEFTLTISSLQPDDFA TYYCFQGSGYPFTFGGGTK		Predominant	
87.36	n.d.			Unknown (487 m/z)		Substantial	New peak
				Unknown (509 m/z) (possibly sodium adduct of 487 m/z)		Substantial	
n.d.	87.55			Unknown			
88.29	88.18	88.26	88.18	DMIFNFYFDVWGQGTTVTVSS ASTK		Predominant	

Appendix B: List of Symbols, Abbreviations, and Acronyms

RM	Reference Material
SRM	Standard Reference Material
5YSV	5-Year Stability Verification
UV	Ultra Violet
DLS	Dynamic Light Scattering
PS	Primary Sample
CE	Capillary Electrophoresis
SEC	Size Exclusion Chromatography
CZE	Capillary Zone Electrophoresis
CE-SDS	Capillary Electrophoresis- Sodium Dodecyl Sulfate
nrCE-SDS	Non-Reducing Capillary Electrophoresis Sodium Dodecyl Sulfate
rCE-SDS	Reducing Capillary Electrophoresis Sodium Dodecyl Sulfate
ANOVA	Analysis of Variance
RA	Relative Abundance
HMW	High Molecular Weight
LMW	Low Molecular Weight
mAb	Monoclonal Antibody
PTM	Post-Translational Modification
FI	Flow Imaging
ECD	Equivalent Circular Diameter
SD	Standard Deviation
LC	Liquid Chromatography
MS	Mass spectrometry
EDTA	Ethylenediaminetetraacetic Acid
DTT	Dithiothreitol
TIC	Total Ion Chromatogram
LOD	Limit of Detection